Effect of Water Temperature on Cohesive Soil Erosion

Olivia Waverly Parks

Thesis submitted to the faculty of the Virginia Polytechnic Institute and State University in partial fulfillment of the requirements for the degree of

Master of Science

In

Biological Systems Engineering

Theresa M. Thompson
W. Cully Hession
Matthew J. Eick

December 12, 2012
Blacksburg, VA

Keywords: cohesive soil, water temperature, erosion rate, zeta potential

Effect of Water Temperature on Cohesive Soil Erosion

Olivia Waverly Parks

ABSTRACT

In light of increased stream temperatures due to urbanization and climate change, the effect of water temperature on cohesive soil erosion should be explored. The objectives of this study are to: determine the effect of water temperature on the erosion rates of clay; determine how erosion rates vary with clay mineralogy; and, explore the relationship between zeta potential and erosion rate. Samples of kaolinite- and montmorillonite-sand mixtures, and vermiculite-dominated soil were placed in the wall of a recirculating flume channel using a vertical sample orientation. Erosion rate was measured under a range of shear stresses (0.1-20 Pa) for a period of five minutes per shear stress at water temperatures of 12, 20, and 27˚C. The zeta potential was determined for each clay type at the three testing temperatures and compared to mean erosion rates. The kaolinite erosion rate doubled when the temperature increased from 12 to 20˚C, and erosion of vermiculite samples tripled when the temperature increased from 20 to 27˚C. The montmorillonite samples generally eroded through mechanical failure rather than fluvial erosion, and the limited fluvial erosion of the montmorillonite-sand mixture was not correlated with water temperature. The data suggest correlation between zeta potential and erosion rate; however, due to the small sample size (n=3), statistically significant correlation was not indicated. Research should continue to explore the influence of water temperature on cohesive soil erosion to better understand the influence of clay mineralogy. Due to the high degree of variability in cohesive soil erosion, multiple replications should be used in future work. The vertical sample orientation enabled discrimination between fluvial erosion and mass wasting and is recommended for future studies.

Acknowledgements

I would like to thank everyone who helped me complete my research. First and foremost, I would like to thank my advisor, Tess Thompson. I would never have come this far without her guidance. I would also like to thank my committee members Matt Eick, and Cully Hession for their advice and support. I thank the BSE department for support over the past few years. My college career would not have been the same without the friends, education, and community gained in BSE.

I would also like to thank Laura Lehman for always being a wealth of knowledge, a supporting hand, and a friend when needed. Laura always goes above and beyond for each struggling graduate student who needs help and should be given a medal of honor for her support and patience.

I am grateful for my family and the support they gave during my time in college. I would especially like to thank my mother for raising me to be a strong, independent woman.

I would like to thank Chris Herman for helping me build the flume wall despite the winter cold, and lack of working tools.

I would like to acknowledge Siavash Hoomehr for his help with ice buckets and other flume activities. I wish him the best of luck with the continuation of this research.

Finally, I would also like to thank Janell Henry, Eric Neuhaus, Karen Hall, and Jeff Garnand-Royo who were always available for advice, encouragement, and a dose of sanity.

Table of Contents

List of Figures

List of Tables

Chapter 1 Introduction

According to the Nation Waters Assessment by the United States Environmental Protection Agency (USEPA) sediment is currently the fifth leading cause of water-quality impairment across the United States (USEPA, 2010). While fine sediment in streams can come from a variety of sources, a leading cause in some watersheds is streambank erosion. While conservation practices have reduced soil erosion from fields, sediment yield in some streams has not decreased due to streambank erosion in the bottomlands of these agricultural sites (Trimble, 2009). Simon et al. (2000) reported that up to 80% of eroded material in incised channels came from the streambanks. Streambank erosion leads to loss of riparian land, and possible damage to stream-side infrastructure such as roads and buildings (Docker and Hubble, 2008). Once sediment is entrained in waterways, it reduces water clarity and decreases the light available to submerged aquatic vegetation. Sediment can also carry toxins and other contaminants, which negatively affect aquatic life and pose health risks for humans (USGS, 2003). Furthermore, sediment in waterways is an economic issue as it increases water-treatment costs, decreases recreational value, and increases the need for dredging of reservoirs or navigable waterways (USEPA, 2008).

Although stream form varies with geology and climate, streambeds are typically composed of non-cohesive material while the streambanks are often composed of cohesive, or fine grained, material. Non-cohesive soil erosion is well understood as the process is predominately governed by the physical properties of the sediment such as shape and particle density; however, the properties and forces that dominate cohesive soil erosion are significantly more complex due to inter-particle attraction between the fine grains (Zhu et al., 2008). While erosion of cohesive soils has been studied, the processes are still poorly understood (Grabowski et al., 2011; Zhu et al., 2008; Zreik et al., 1998).

Because streambank erosion can have a strong influence on water quality, research is needed on the factors that influence cohesive soil erosion rates, particularly stream temperature. Previous research has shown that loss of forested riparian buffers, urbanization, and climate change can increase stream water temperatures by as much as 7˚C (Kozarek, 2011; LeBlanc et al., 1997; Nelson and Palmer, 2007; Stefan and Sinokrot, 1993; Van Buren et al., 2000). Therefore, it is important to understand the influence of stream water temperature on the erosion

of cohesive soils to inform watershed management. The effect of water temperature on cohesive soil erosion may provide insight into the mechanisms which govern the interactions between fine-grained particles, a subject which is currently poorly understood.

Goals and Objectives

The overall goal of this research was to determine if increases in water temperature increased erosion rates of cohesive soils. To achieve this goal three main objectives were completed:

1. Determine if water temperature has a significant effect on the erosion rates of clays;
2. Determine if the influence of water temperature varies with clay mineralogy; and,
3. Examine the relationship between zeta potential, temperature, and erosion rate.

Chapter 2 Literature Review

The following literature review begins by discussing the current and predicted changes to stream water temperatures due to loss of forested riparian buffers, climate change, and urbanization. Subsequent sections discuss clay mineralogy, electric double layer theory, and cohesive soil formation. Finally, the literature review covers factors which affect cohesive soil erosion, especially the current research regarding water temperature influences on erodibility.

Changes in Stream Water Temperature

Urbanization, loss of riparian buffers, and climate change have all been shown to affect stream water temperature regimes (Kozarek, 2011; LeBlanc et al., 1997; Nelson and Palmer, 2007; Stefan and Sinokrot, 1993; Van Buren et al., 2000). Forested riparian buffers shade streams from excess radiation during daylight hours and insulate the stream at night, thus buffering the daily temperature changes of the stream (LeBlanc et al., 1997). Kozarek (2011) compared stream water temperatures between similar forested and nonforested streams and found that the nonforested streams typically had 1-2°C higher average daily temperatures compared to forested streams. Additionally, the nonforested streams exceeded the Pennsylvania state water temperature standard (30.6°C) several times over the summer monitored but this standard was never exceeded in the forested streams. LeBlanc et al. (1997) also showed, through modeling, that removal of riparian vegetation led to increases in stream temperatures of up to 2°C.

In addition to loss of riparian vegetation, urbanization leads to changes in flow regimes and channel morphology, as well as thermal pollution from stormwater runoff and industries (LeBlanc et al., 1997; Nelson and Palmer, 2007; Van Buren et al., 2000). LeBlanc et al. (1997) modeled changes in stream temperature regimes due to urbanization by adjusting three model parameters: decreases in riparian vegetation; decreases in base flow; and, enlargement of channel geometry. These combined changes predicted a 4˚C rise in peak stream temperature for a typical summer day in Ontario, Canada. The rise in stream temperature was expected to increase if the modeled contributions of groundwater inputs to the stream were decreased. LeBlanc's model, however, ignored the rise in runoff temperature which can occur as stormwater runs over hot pavement in urban centers. While urban centers are designed to efficiently convey stormwater

away from the city and into streams, this efficiency enhances the effects of urban thermal pollution by delivering heated waters more rapidly to receiving streams (Van Buren et al., 2000). Nelson and Palmer (2007) measured the effects of summer storm runoff on stream water temperature surges. Storms in urbanized areas (20-50% impervious surfaces) frequently caused surges in stream temperatures which averaged 3.5°C and lasted about 3-hr before dissipating. Storm surges increased stream temperatures by over 7°C at some monitored sites.

Climate change is also expected to cause a temperature rise in US streams, with changes most evident during low flow; some stream temperatures have already begun to increase (Backlund et al., 2008). Based on the general circulation model, when twice the amount of current CO_2 has been released into the atmosphere, the average air temperature is expected to rise 4.5°C (Mohseni et al., 1999). Under this condition, average summer stream temperatures are predicted to rise 2-5°C due to increased air temperature, changes in precipitation, and a decrease of ground cover due to harsher growing climates (Backlund et al., 2008; Mohseni et al., 1999; Stefan and Sinokrot, 1993). Mohseni et al. (1999) modeled a range of temperature changes from 2-13°C across the United States; stream temperatures in Louisiana were predicted to reach an average temperature of 30°C during the hottest weeks. The combination of urbanization and climate change will certainly lead to considerable changes in stream temperature regimes.

Cohesive Soils

Cohesive soils are ubiquitous in most riverine systems (Grabowski et al., 2011); however, the precise definition of cohesive soils is difficult to specify. These soils have a high percentage of fine-grain particles (i.e., clays, silt) which dominate the physical and chemical properties of the soil. The primary component of cohesive soils is clay minerals which are formed through weathering processes and are less than 2 μm in diameter (Grabowski et al., 2011). The small size of clay particles leads to inter-particle attraction or cohesion. These complex attraction forces are an essential characteristic of cohesive soils and differentiate these soils from non-cohesive soils, which exhibit little to no attraction between particles (Zhu et al., 2008).

Clay Types and Properties

Clays are a product of the weathering of silicate minerals in the soil (e.g., mica, quartz, feldspar, etc.) and typically occur as layer silicates. Clay minerals are primarily classified by the

number of tetrahedral (silica) and octahedral (typically alumina) sheets and by isomorphic substitutions within the layers. Isomorphic substitution occurs when a cation in the mineral structure is replaced by another cation of similar size, such as Mg^{2+} for Al^{3+}, which leads to a negative charge in the structure. The most basic clay is constructed from one tetrahedral sheet and one octahedral sheet and is referred to as a 1:1 clay. The adjacent layers of 1:1 clays are generally bonded by hydrogen bonds which inhibit expansion. Clays with two tetrahedral sheets sandwiching one octahedral sheet are called 2:1 clays. The 2:1 clays can be further classified by the degree and location of isomorphic substitutions; the isomorphic substitutions also affect the strength of attraction between layers and the ability of a clay to hydrate and expand (McBride, 1994).

Four dominant types of clay minerals include kaolinite, smectite, illite, and vermiculite (Grabowski et al., 2011; Zhu et al., 2008). These four clays each exhibit differences in porosity, cation exchange capacity (CEC), expansion, plasticity, water adsorption, and erodibility due to variation in structure (Table 2.1) (Brady and Weil, 2008; Grabowski et al., 2011). Figure 2.1 depicts the basic structure of these four clay types. Kaolinite is a 1:1 clay which has little isomorphic substitution and consequently low surface charge. Illite, a 2:1 clay, is the weathered form of mica. While this clay has a high negative surface charge, potassium cations are fixed between the clay layers and lead to strong interlayer bonding and little expansion and CEC. Conversely, montmorillonite is a 2:1 smectite clay with relatively low interlayer bonding strength, which gives montmorillonite a large capacity to adsorb water between the clay layers. While vermiculite is also a 2:1 clay, it has a greater layer charge than montmorillonite which limits the expansion between clay layers, but gives vermiculite the highest CEC of all clays. This clay is considered semi-expanding (Brady and Weil, 2008; McBride, 1994).

Table 2.1 Comparison of clay types (Brady and Weil, 2008; Grabowski et al., 2011).

Classification	**Size, μm**	**CEC, $cmol_c/kg$**	**Plasticity**	**Cohesion**	**Expansion**
Kaolinite	0.1-0.5	1-15	Low	Low	Non-expanding
Illite	0.2-2.0	10-40	Medium	Medium	Non-expanding
Vermiculite	0.1-0.5	100-200	Medium	Medium	Semi-expanding
Montmorillonite	0.01-1.0	80-150	High	High	Fully-expanding

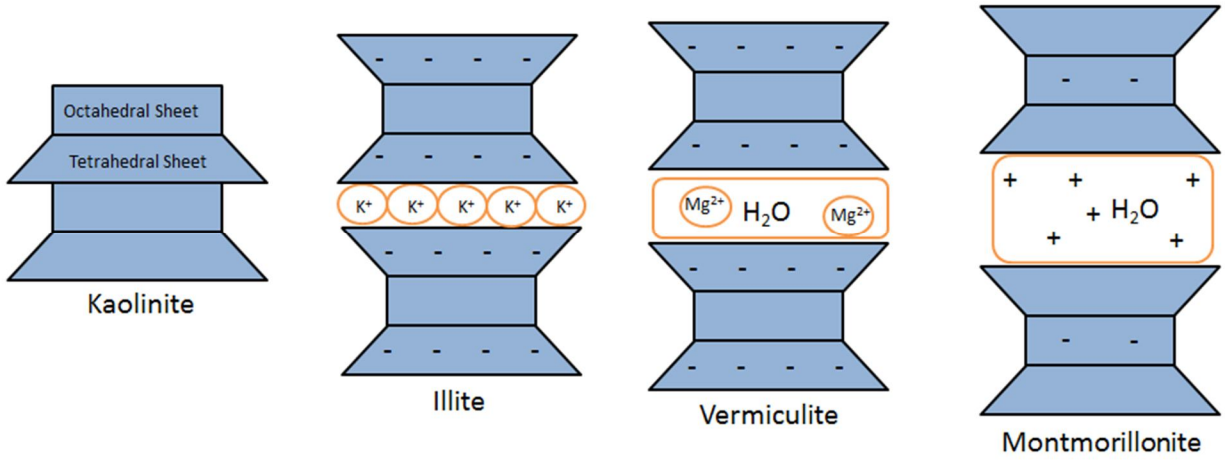

Figure 2.1 Schematic of dominant clay types with structural charge (-) and cations (+) indicated; adapted from McBride (1994) and Brady and Weil (2008).

Electric Double Layer Theory and Zeta Potential

Electric double layer (EDL) theory was developed to explain the location and distribution of exchangeable cations near the surface of clay sheets (McBride, 1994). Cations in solution (counterions) are attracted while anions (coions) are repelled by the negative surface charge of clays. Surface charge can be classified into two categories: structural charge and variable charge. Structural, or permanent, charge is developed by isomorphic substitutions in the mineral structure. Variable, or pH-dependent, charge is formed by weakly acidic functional groups attached to the mineral surface which can protonate or deprotonate depending on the pH (McBride, 1994). The EDL begins at the negatively charged clay surface; the inner, or Stern, layer is a thin layer of cations that are specifically absorbed to the clay surface. The outer diffuse, or Guoy, layer is comprised of counterions that are electrostatically attracted to the surface and devoid of coions that are negatively adsorbed or repelled by the surface (Figure 2.2) (Laird, 2006; McBride, 1994; Shang et al., 1994). It is the charged clay surface and the unequal distribution of counter- and coions compared to the bulk solution that comprise the EDL. The EDL is important to understanding the behavior of clays. Flocculation or dispersion in colloids, hydraulic conductivity, and swelling are all influenced by the EDL (McBride, 1994; Shang et al., 1994). For example, as the EDL expands, particle repulsion increases, increasing the tendency of

particles to remain in suspension; however, if the double layer decreases in size, the particles become less dispersed and are more likely to flocculate (McBride, 1994).

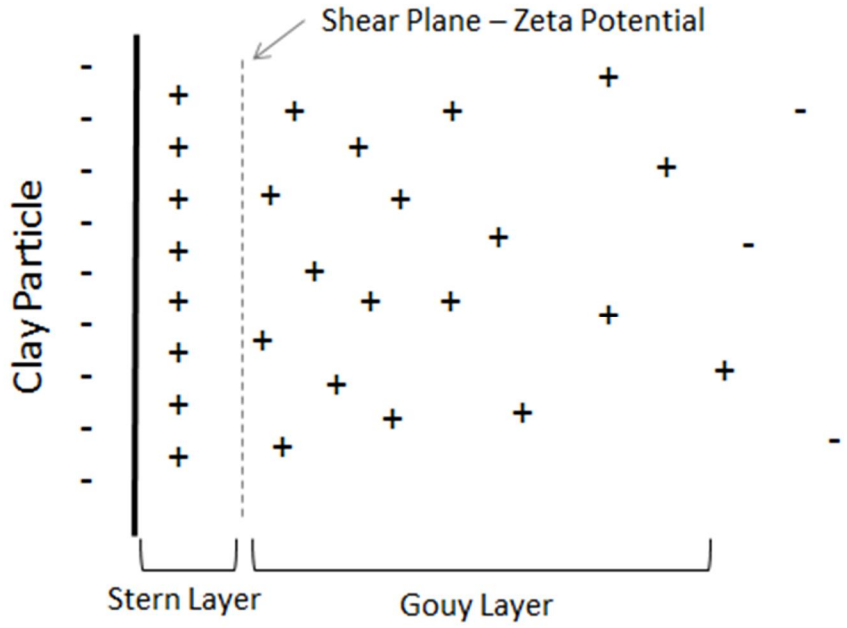

Figure 2.2 Depiction of electric double layer (EDL); adapted from Shang et al. (1994).

The charged mineral surface and associated counter- and coions (Gouy or diffuse layer) that neutralize the surface creates an electropotential between the surface of the colloid and any point in the diffuse layer. This voltage difference is on the order of millivolts and is refferred to as the surface potential of the colloid. The magnitude of the surface potential is related to the thickness of the EDL and the surface charge of the colloid. While the EDL or surface potential of clays cannot be directly measured, it is common practice to measure the zeta potential, which can then be used to approximate surface potential (Shang et al., 1994). The zeta potential is measured at the boundary between the Stern layer and diffuse layer (shear plane). Zeta potential can be quantified by tracking the particle as it migrates in a charged field (electrophoresis) (Figure 2.2) (McBride, 1994). The exact location of the shear plane is debated; traditionally the shear plane is located just beyond the Stern layer, but the shear plane could also be located

farther into the Gouy layer depending on which model of double layer theory is used (Li et al., 2003; Shang et al., 1994). Zeta potential gives insight to the electrokinetic properties of minerals and has been used to determine potential flocculation/dispersion of particles, and to describe rock-fluid interactions in the oil refinement industry (Baumgarten et al., 2012; Ramachandran and Somasundaran, 1986). Zeta potential can be used to predict the stability of clay particles in suspension using the following guidelines: values from -40 to -31 mV are in stable dispersion; values of -4 to +3 mV are strongly aggregating and possibly experiencing sedimentation; values between -30 to -4 mV exhibit low to medium aggregation (Baumgarten et al., 2012). As zeta potential is a measure of inter-particle attraction, it is believed that zeta potential could be related to the erodibility of cohesive soils.

Cohesive Soil Formation

While it is ideal to study the properties of pure clay samples; typically, cohesive soils are comprised of a complex mixture of clays due to difference in weathering rates and microclimates. Additionally, natural soils also contain sands, silts, and organic matter; all of which interact to form soil structure (Figure 2.3) (Baumgarten et al., 2012; Grabowski et al., 2011). Soil structure begins as clay particles flocculate to form small clumps, that are held together by the attraction of cations to negatively charged clay surfaces (Brady and Weil, 2008). As previously stated, flocculation generally occurs at a decreased EDL, when repulsion between clay particles does not inhibit inter-particle attraction (McBride, 1994). Clumps are then attracted to each other as positive clay edges are attracted to other negative clay surfaces. When many clumps bind to each other and to fine silts, microaggregates are formed (2-250 μm in size). Macroaggregates (0.25-5 mm) form due to attraction between microaggregates, cementing effects of oxides, and biological processes (Brady and Weil, 2008; Edwards and Bremner, 1967; Grabowski et al., 2011).

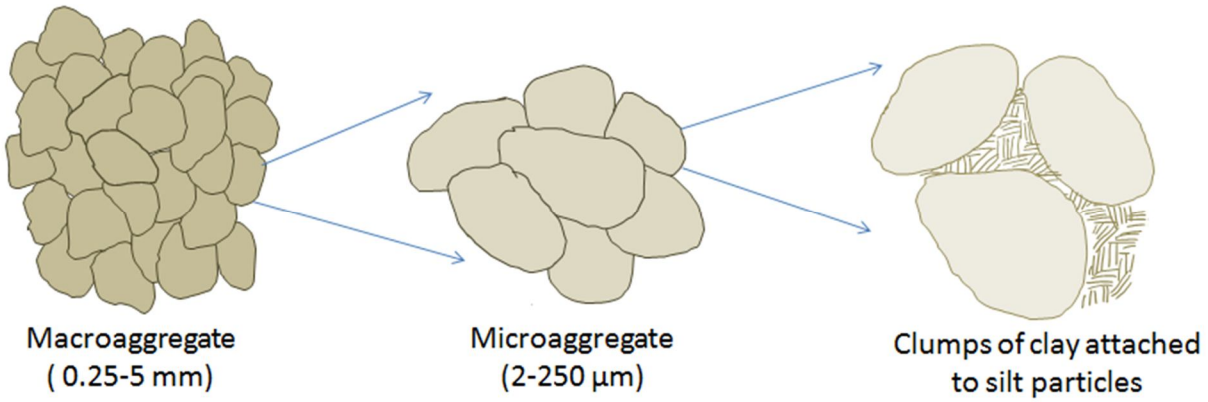

Figure 2.3 Cohesive soil formation; adapted from Brady and Weil (2008)

Biological processes play a large role in the formation of soil structure. At the smallest scale, microorganisms, polysaccharides, and other organic compounds all act as binding agents to hold microaggregates together. On a larger scale, plant roots and animal burrows push soil particles together creating more defined soil structure. Soil structure is also influenced by wet/dry and freeze/thaw cycles. As soil water is withdrawn from a soil, or the soil is compressed during freezing, the clay particles move closer together and cracks form along planes of weakness. After many cycles, the cracks become more pronounced, creating a defined soil structure (Brady and Weil, 2008; Grabowski et al., 2011). A soil ped (few mm to 1 m) represents the large scale soil structure but generally has low tensile strength. Peds can be easily broken along natural zones of weakness because the particles in macroaggregates are more strongly attracted to one another than to other aggregates. Burrows, macropores, and weak cracks caused by freeze/thaw and wet/dry cycles also decrease the strength of soil peds (Brady and Weil, 2008).

Cohesive Soil Erosion

Erosion occurs as bonds between macroaggregates, microaggregates, and/or particles are overcome by an external force, such as hydraulic shear stress (Grabowski et al., 2011; Thorne et al., 1998). Cohesive soil erosion is a factor of both soil properties and environment. Soil composition is the primary factor in soil erosion resistance. Increased clay content increases soil erosion resistance (Kamphuis and Hall, 1983; Zhu et al., 2008). Additionally, the type of clay mineral affects the erosion resistance due to differences in mineral structure and inter-particle

bonding as seen in the different levels of cohesion between clay minerals (Table 2.1) (Gaskin et al., 2003; Grabowski et al., 2011; Grissinger, 1966). On a larger scale, increased bulk density and soil consolidation have been shown to increase erosion resistance (Grissinger, 1966; Kamphuis and Hall, 1983). An increase in soil consolidation decreases inter-layer spacing which increase inter-particle bonding and erosion resistance (Kamphuis and Hall, 1983). The natural soil structure affects erosion rates as the cracks and fissures within a soil creates planes of weakness (Gaskin et al., 2003). Since erodibility is highly dependent on the type and amount of clay involved, it is unfortunate that few studies describe the specific mineralogy of the samples used during experimentation (Grabowski et al., 2011; Zhu et al., 2008).

Environmental influences on soil erosion include: wetting and drying cycles; desiccation; freeze and thaw cycles; water salinity, temperature, and pH; soil moisture content; and time (Grissinger, 1966; Kamphuis and Hall, 1983; Raudkivi and Hutchison, 1974; Thorne et al**.,** 1998). The natural soil structure, partially defined by processing of wetting and drying, freeze and thaw, and dessication, generates zone of weakness (Gaskin et al., 2003; Thorne et al., 1998). Cohesive soil erodibility is also time-dependent. As a soil is initially wetted, the erosion resistance will decrease as the water enters inter-layer spaces and breaks inter-particle bonds; however, as saturation time elapses, the free water is absorbed, the soil hydrates, and stronger bonds between particles are created (Thorne et al., 1998). When dealing with remolded samples in a laboratory experiment, the aging time of a sample can greatly affect soil erosion resistance as inter-particle bonds need time to form (Grissinger, 1966). The salinity of the eroding water also affects erosion rates of clays. Raudkivi and Hutchison (1974) observed that an increase in salinity led to increased cohesiveness for kaolinite soil samples thus increasing erosion resistance. The form of fluvial action, such as waves or currents, on a sample will also affect erosion rates (Gaskin et al., 2003).

Temperature Effect on Cohesive Erosion

While prior studies have shown that water temperature has an effect on erosion, few, if any, experiments have directly studied the process for different clay types or for streambank erosion (Grabowski et al., 2011). Table 2.2 summarizes experiments examining the effect of water temperature on soil erosion. In these flume studies, the soil sample was placed in the bed of the flume. Researchers typically used remolded, natural soil with clay amendments. Methods

of soil consolidation differed between experiments; most commonly the sediment was deposited out of a slurry, but compacted, and remolded samples were also used. Typically water temperature, ranging from 15-40°C, was kept constant during the experiment.

Several studies were not initially testing the effects of water temperature on erosion, but rather noticed that the water temperature influenced the experiment (Grissinger, 1966; USDI, 1963; Zreik et al., 1998). While testing the critical shear strength of earth-lined canal channels, the researchers of the USDI (1963) noticed that erosion rate varied with water temperature and calculated an increase in critical boundary shear stress of 0.0036 lb/ft^2 per ˚C (0.17 Pa/˚C) which is the opposite effect seen by other researchers. However, this conclusion from the USDI research was drawn from testing only one soil sample at three temperatures without any replication. Zreik et al. (1998) also monitored water temperature during experimentation and noticed that a sample at 29˚C eroded more than a sample at 20˚C. However, the temperature only influenced the top 0.5-mm of sample, beyond which the soil strength, determined by an Automated Fall Cone Device, and age of the sample were the dominant factors affecting erosion rate. Zreik et al. (1998) believed that the decrease in erosion resistance was caused by a decrease in bond strength at higher temperatures. The concept that bond strength is affected by water temperature was further explored by other researchers (Kelly and Gularte, 1981; Raudkivi and Hutchison, 1974) and is discussed in greater detail under '*Modeling Cohesive Erosion.'*

The research of Taylor and Vanoni (1972) focused on the effect of water temperature on erosion for different hydraulic regimes. Research was conducted in a recirculating flume with a loosely packed sediment bed; different grain sizes were tested separately. Their results indicated that the effect of water temperature depended on the relative hydrodynamic roughness of the bed, where roughness was determined by Reynolds number. For fully rough flow, such as flows over a gravel bed (D_g=3.95 mm) or coarse clay aggregates (D_g=18.5 mm), temperature had no influence on sediment discharge. In the lower transitional range, which occurred when the bed was comprised of fine sand grain particles (D_g=0.14-0.36 mm), an increase in temperature increased the sediment discharge and decreased the mean bed shear stress. However, in the upper transitional regime, as seen with a sandy bed (D_g=1.07 mm), water temperature had the opposite effect. These experiments did not include tests on fine clay bed material or hydrodynamically smooth flows. The results suggest that the effect of temperature is strongly related to grain size. Due to the grain sizes used, these results are only directly applicable to non-cohesive sediments.

Table 2.2 Summary of previous research on cohesive soil erosion and water temperature

Article	Soil Type	Sample Preparation	Water Temperature, °C
USDI (1963)	Unspecified soil with 44% clay	Brought to and unspecified moisture content and bulk density, submerged for 48 hours	18.2, 27, 32
Grissinger (1966)	Grenada silt loam, 20% clay including kaolin, montmorillonite, vermiculite, illite, and some amorphous material.	Added fine, medium, and coarse grade kaolinite; Na- and Ca- montmorillonite; and, Fithian illite. Processed through mill to removed aggregates, moistened to 5- 20% MC, compacted to desire bulk density of 1.3-1.6 g/cm^3.	Obsevered influence when water temperature fluctuated. Consequently restricted water temperature to 25 ± 2
Taylor and Vanoni (1972)	Clay aggregates (D_g = 18.5 mm), Fine silica sand (D_g=0.14-0.36 mm), fine gravel (D_g=3.95 mm), and coarse sand (D_g=1.07 mm), all tested separately	Loosely packed into a flatbed form	20.5 - 63, but primarily 20 - 40
Christensen and Das (1973)	Kaolinite, Grundite, Kaolinite+sand, and Grundite+sand.	Packed to line a brass tube.	12.5 - 40
Raudkivi and Hutchison (1974)	English kaolinite (<1 µm) Georgia kaolinite (2-5 µm and 5-8 µm)	Mixed in a slurry and consolidated—still fluid after consolidation.	16 - 32
Kelly and Gularte (1981)	Grundite (illite clay)	Remolded by mechanical mixer and placed in a support tray	10, 15, 20, 25, 30
Zreik et al. (1998)	Boston Blue Clay	Deposited from suspension in distilled water, then left to settle for 2-19 days	20, 24, 26, 28, 29

In general, all studies in Table 2.2 indicated that increasing water temperature increased erosion of cohesive soils. However, these studies were directed toward erosion from the stream bed, which involves both sediment detachment and entrainment. Contrary to bed erosion, near-vertical streambanks only require particle or aggregate detachment for erosion to occur, which simplifies the process and increases the amount of erosion predicted to occur since the energy needed for entrainment is not required. When positioned in a stream bed, the force of gravity on the soil particle directly opposes the hydraulic forces; during streambank erosion, the effect of gravity is lessened due to the bank angle. Additionally, the experimental set-up of many of these experiments would not be representative of a natural streambank due to a lack of compaction and consolidation of the soil samples. Results from these studies cannot be readily translated to streambank erosion processes, especially since the effect of water temperature on erosion rates was not quantified.

Modeling Cohesive Erosion

Thus far, modeling of cohesive erosion has proven quite difficult due to the complex relations between soil properties and stream environments. In general it is understood that erosion begins once a certain threshold has been reached and the resisting forces are overcome by the erosive forces. Partheniades (1965) determined that erosion occurred once an excess shear stress was reached at the soil surface. Under this principle, erosion increases with increasing shear stress, but only after a critical shear stress has been reached. A general equation to describe erosion was described by Moody et al. (2005):

$$E = KX \tag{1}$$

where: E = erosion of soil particles per unit area per unit time;
K = soil erodibility; and,
X = a hydraulic flow parameter.

Soil erodibility is dependent on both the soil properties and the environment. An example of a hydraulic parameter, X, would be a function of the shear stress on the soil surface (Partheniades, 1965).

Other authors have speculated that cohesive soil erosion is controlled by rate process theory (Christensen and Das, 1973; Kelly and Gularte, 1981; Raudkivi and Hutchison, 1974). With this theory, erosion begins once the activation energy of the system is exceeded, or when there is enough energy to break the inter-particle bonds. Rate process theory relates erosion rates and the temperature of the system since the temperature influences the electro-chemical bond strength (Parchure and Mehta, 1985).

When applied to erosional processes, the rate process theory can be written as (Kelly and Gularte, 1981):

$$\varepsilon = x\frac{kT}{h}\exp\left(-\frac{\Delta F}{RT}\right)\exp\left(\frac{\tau V_f}{2kT}\right) \quad (2)$$

where: ε = the erosion rate;
x = a constant;
k = Boltzmann's constant;
h = Plank's constant;
T = absolute temperature;
ΔF = activation energy;
R = universal gas constant;
τ = hydraulic shear stress; and,
V_f = experimental flow volume.

Kelly and Gularte (1981) tested the rate process theory by calculating erosion rates for remolded illitic silt under different temperatures (15-30˚C) at the same shear stress. Samples were also tested at different salinities (2.5-10 ppt NaCl) and water content (40-80%). Experiments resulted in an overall rise of erosion rates with increased temperature. Based on the calculated activation energy, it was concluded that the inter-particle bonds behaved as a solid-to-solid bond which had little dependence on moisture content or salinity. However, these experiments were conducted with samples located in the bed of the flume. In this position, both detachment and entrainment were necessary for erosion to occur, which increases the energy needed to produce erosion. If the samples were located in a streambank position, such as this study, the activation energy, and thus bond-strength might have been drastically lower.

Raudkivi and Hutchison (1974) also found that erosion rate increased with increasing water temperature (16-32˚C). Raudkivi speculated that the increase in erosion rate was related to the amplitude of water particle vibrations. As the temperature is increased, the water particles interacting with the soil surface experience greater vibrations, causing the surface particles to also increase in vibration. As the amplitude of vibration increases for the soil surface particles, inter-particle cohesive bonds are weakened, thus increasing the likelihood to erosion. However, the soil particle detachment may not be influenced by water temperature if the cohesive bonds are sufficiently strong enough to withstand the increase in amplitude. Overall it is believed that physio-chemical forces rather than mechanical forces were controlling surface erosion. These results indicate that, due to the nature of attraction between clay particles and the agreement with rate process theory, there is a relationship between water temperature and soil erosion rates (Kelly and Gularte, 1981).

In summary, the current understanding of cohesive soil erosion is inadequate. There are many factors which affect cohesive soil erosion including clay mineralogy, environmental conditions, and soil structure. By narrowing the variables studied, the effect of individual factors can be better understood. As stream temperatures rise due to urbanization and climate change, studies should focus on the effect of water temperature on cohesive soil erosion as previous research has indicated an increase in erosion with increased water temperature.

Chapter 3 Methods

To test the effect of water temperature on the erosion of cohesive soils, remolded soil cores were placed in a flume wall and subjected to a series of shear stresses. The process was repeated at average water temperatures of 12, 20, and 27˚C. Erosion rate was measured by tracking the advancement of the sample necessary to keep the sample flush with the wall. Statistical analyses were used to determine significant differences in average erosion rates for the different samples at different water temperatures.

Flume Set-up

An 8 m x 1 m x 0.4 m recirculating flume (Engineering Laboratory Design, Lake City, MN) was used to conduct the experiment. An artificial wall was created in the channel to narrow the channel width to 40 cm and to decrease the volume of water needed to run the flume to roughly 3700 L. The wall was created from 1.25-cm thick PVC sheeting with a wooden structure for support. At the flume entrance, thin plexiglass was used to create a curved wall to narrow the channel gradually. A honeycomb flow straightener was also positioned at the channel inlet. The artificial wall also allowed the experiment to simulate a streambank setting by placing the core in the wall (Figure 3.1); in this position only detachment is needed for erosion to occur. This position also allowed erosion to occur as fluvial erosion or mass wasting. In prior research, samples were placed in the flume bed, in which case both detachment and transport are necessary to move the soil particles (Kelly and Gularte, 1981; Raudkivi and Hutchison, 1974; Taylor and Vanoni, 1972; Zreik et al., 1998). By placing the sample in a vertical position, the dominant mode of soil loss, fluvial erosion or mass wasting, can be distinguished. Mass wasting cannot occur in a flume bed setting.

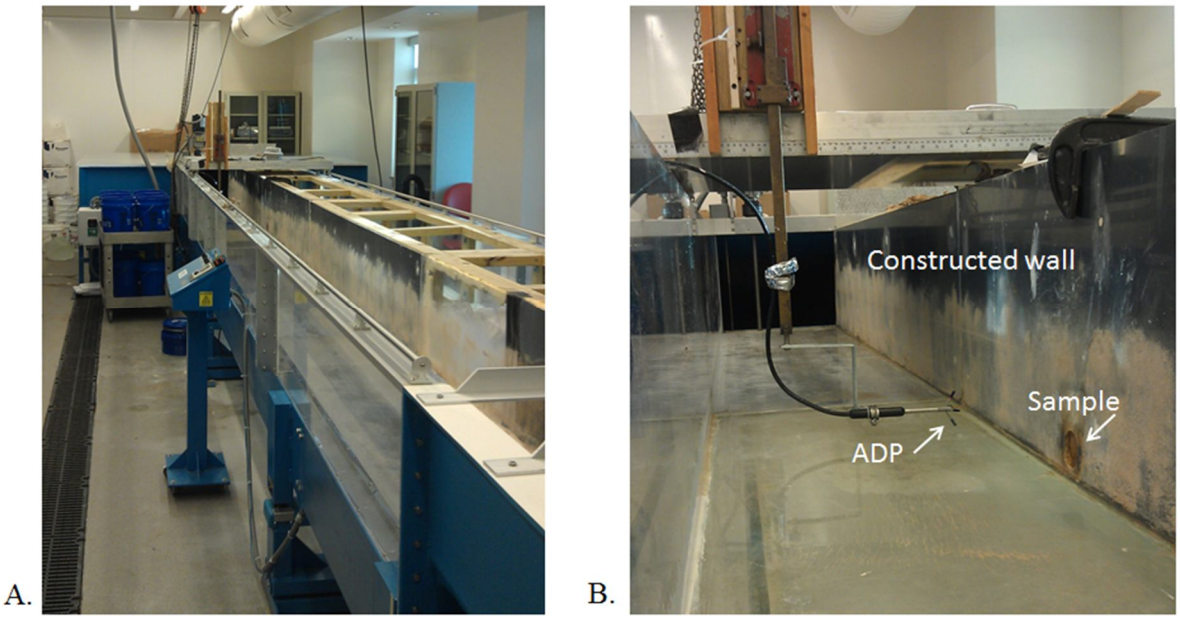

Figure 3.1 A. Flume channel; B. Close-up of sample position

To determine the best location for the soil core placement, velocity profiles were measured down the center of the test section, and normal to the wall at varying depths with a Vectrino II acoustic Doppler profiling (ADP) velocimeter (Nortek AS, Vangkroken, Norway) at multiple flow conditions. The ADP measures velocities in three dimensions over a 2-cm range located 4 cm from the probe head; measurements are taken in 1-mm intervals, or bins, throughout the sampling range at a rate of 50 Hz. The probe head was placed in a horizontal position (Figure 3.1B) to collect a centerline velocity profile perpendicular to the wall. Seven flume settings were selected which produced uniform flow in the test section, as determined using velocity profiles (Table 3.1). Law of the wall was used to determine the boundary shear stress for these seven settings.

The sample was placed 74 cm into the flume test section, or 5.24 m from the channel inlet as this position experienced minimal headwater or tailgate effects at all seven shear stresses. The center of the sample was located 4.5 cm from the flume bed (Figure 3.1), which was low enough to completely submerge the sample at the lowest flow depth and still accommodate the depth needed for the ADP probe. The sample support bracket was designed so the core could be advanced from behind the constructed wall in 1-mm increments (Figure 3.2). Soil advancement kept the sample flush with the wall after erosion events to minimize form drag on the sample

surface. To compensate for the roughness of the sample surface, and to allow full development of the wall boundary layer, sand was adhered to the constructed wall surface with spray adhesive. The sand (Premium Play Sand No. 1113, Quikrete, Atlanta, GA) had a D_{50}=0.15 mm and a D_{84}=0.3 mm.

Table 3.1 Flume setting series used for each testing replication

Setting	Tailgate height, cm	Channel Slope, %	Flow Depth, cm	Flow rate, m^3/s	Wall shear stress* τ_o, Pa
1	10	0.5	14	0.017	0.2
2	5	0.5	9	0.017	0.5
3	5	0.5	13	0.036	0.7
4	0	0.5	9	0.036	3.0
5	0	0.5	10	0.055	4.0
6	0	1.0	8	0.055	6.5
7	0	1.5	7	0.055	7.0

* As determined at center of the sample

Figure 3.2 Sample support bracket and advancer with graduation markings used to advance soil sample and track erosion

Sample Creation

Three clay types, kaolinite, vermiculite, and montmorillonite, were chosen to represent a range of clay properties (Table 2.1). The kaolinite was filler-grade kaolinite with at least 85% of particles less than 2 μm (B-80, Thiele Kaolin Company, Sandersville, GA). The montmorillonite clay used was 325-mesh calcium montmorillonite clay powder (Greenclays.com, Las Vegas, NV). A natural soil was used for vermiculite samples. The natural soil (Ross Soil--Cumulic Hapludoll, fine-loamy, mixed, mesic) was acquired from the top 10-40 cm of a river terrace located next to the New River at Whitethorne, VA. This soil was previously characterized as 20.4% clay, 40.2% sand, and 39.4% silt. The clay fraction of the natural soil was comprised of 35% hydroxyl interlayered vermiculite, 10% vermiculite, 10% mica, 15% kaolinite, 13% quartz, 10% chlorite, and 6% smectite (Harris et al., 1980). The natural soil was air dried, pulverized using a mortar and pestle to remove the macrostructure, and passed through a 2-mm mesh.

For each clay type, multiple combinations of bulk densities and percentages of clay and sand were tested to determine a mixture that would erode under the highest shear stress setting, but also had sufficient soil strength and cohesion to withstand sitting in still water without mass wasting. It was found that 100% clay samples would not eroded under the highest shear setting, so sand was added to the mixture. For the montmorillonite mixture, the samples were also limited by the hydraulic conductivity of the soil core; dense samples with high clay content could not be saturated throughout the core due to swelling.

When making each core the air-dried mass of clay was weighed out first; moisture content of the air-dried samples was accounted for when determining clay mass needed. Based on the initial erosion tests, the appropriate amount of oven-dried sand (Premium Play Sand No. 1113, Quikrete, Atlanta, GA) was added to the clay. To make compaction easier, 10-25 g of deionized (DI) water was added. The mixture was thoroughly stirred until a uniform consistency was achieved. The mix was then poured into a 5 cm tall, 5-cm diameter aluminum ring and compacted with a slide hammer (4.64 kg) by raising the hammer and allowing it to fall freely. Hammering was continued until the desired bulk density was reached. If two layers were needed to achieve the target bulk density, the upper surface of the first layer was roughened before adding more sample. Specifics of the soil core properties and creation process are shown in Table 3.2.

Table 3.2 Specifications for sample creation in a 5-cm dia. ring using a slide hammer.

Clay type	Bulk density g/cm^3	Percent clay, %	Clay moisture content before mixing, %	DI water added, g	No. of layers	Hammer blows per layer
Kaolinite	1.4	60	0.8	25	2	2
Vermiculite	1.5	20.4*	7.5	20	2	3
Montmorillonite	1.3	30	4.7	10	1	3

* Used a natural soil

Once created, the cores were soaked overnight in DI water. A mesh fabric was placed over the top and bottom of the core to maintain structure while allowing water to permeate the core. The saturated cores were then placed on a pressure plate (5 Bar pressure plate extractor cat. #1600, Soilmoisture Equipment Co., Santa Barbara, CA) at vacuum pressure of 1/3 bars, or 4.3 psi for a period of no less than three days (typically 3-5 days) to bring the samples to field capacity. Once removed from the pressure plates, samples were stored in a sealed glass jar over a layer of water to create a 100% humidity micro-climate to maintain the moisture content of the samples. Samples were stored in the glass jar for 0-4 days prior to testing. The time from core creation to use in testing ranged from 4-9 days.

Testing Method

Testing began by setting the flume to the lowest shear stress setting. Then a sample core was placed into the soil advancer system within the flume wall and advanced until the sample protruded from the wall approximately 3 mm. The sample advancer was marked with 1 mm graduations, and the initial and final positions of the pusher were recorded for each test. The protruding sample was shaved flush with the wall using a cheese wire. A picture was taken to record the sample surface prior to testing. The sample was covered with a plastic tray which prevented substantial shear stress on the sample, but allowed the sample to wet while the flow was developed. Once uniform flow was achieved (50-130 s), the sample was uncovered and the ADP was turned on to begin data collection. Using the bottom distance measurement from the ADP, sample erosion was recorded every 0.1 seconds. The precision of the bottom distance measurement depends on the flow conditions and the measurements varied from the mean by an average of 0.01 to 0.27 mm, with a maximum deviation of 0.64 mm. The initial bottom distance

reading was recorded as the neutral position; erosion was assumed to occur when the bottom distance reading was 1 mm past the neutral position. The sample was advanced following each 1 mm of erosion to keep the sample flush with the wall. The time of 1 mm erosion, and time of each sample advancement was recorded.

For each flume setting, the sample was subjected to flow for 5 min at (Table 3.1). If the sample did not erode 1 mm after 5 min, the sample was covered, the flume channel was drained, and a picture was taken. If 1 mm erosion occurred, soil advancement/erosion was monitored for 5 min before the sample was covered, the flume channel was drained, and a picture was taken. After each setting, the sample was again advanced and shaved flush with the wall to prepare a fresh surface for the next higher shear stress (Table 3.1). Two soil cores were created for each soil type and water temperature treatment; the second soil core was used if the first core was completed eroded. The process was repeated for all seven pre-determined flume settings (Table 3.1), or until both cores were used. Three replicates were run for each soil type and for each temperature setting. Soil cores were tested at temperatures of 10.4-13.5, 19.1-21.8, and 26.9-28.4˚C. To cool the flume water, buckets of ice were placed in the tank prior to testing; additional ice was added between replicates to compensate for heating of the water as it moved through the pumps. Tap water from the Blacksburg-Christiansburg-VPI Water Authority was used to fill the flume and for all ice. Two 1000-W aquarium heaters (True Temp T-1000, Transworld Aquatic Ent., Inglewood, CA) were used to heat the water.

A 250-mL sample of water was taken during the second replicate testing to find average total suspended solids (TSS) of the flume water. Grab samples were collected from the center of the flume channel while the channel was draining after a 5-min shear stress setting. One sample was taken from the tank waters after the third replicate. Sample were kept frozen until tested. TSS was determined by passing a 100-mL sample of water through a 0.7-µm Whatman glass fiber filter (GF/F) following the EPA 160.2/SM 2540 D method for a vacuum system (Cesceri et al, 1998).

Zeta Potential

A Zetasizer 3000HS (Malvern Instruments, Worcestershire, UK) was used to determine the zeta potential for each clay type at water temperatures of 12, 20, and 27˚C. A dilute suspension was created for each soil type in DI water. For the natural soil sample, the suspended

solution was allowed to settle slightly so that Fe oxides settled out and only the phyllosilicate minerals were tested.

Data Analysis

Erosion rate and shear velocity for each run was calculated. The first millimeter of erosion was disregarded so a definitive erosion start time could be determined. Erosion rate was calculated by dividing the total advancement after the first 1 mm of erosion by the time between 1 mm of erosion and the end of testing for each 5-min run. Any event where the core eroded more than 2 mm over 5 s was classified as a mass wasting event and was not included in erosion rate calculations. Velocity profile data from the ADP were used to determine the shear velocity for each run using the rough equation for law of the wall (Kundu, 1990):

$$u(y) = \frac{u*}{k} \ln\left(\frac{y}{yo}\right) \quad (3)$$

where: u(y) = streamwise velocity at distance y from the wall, m/s;

u* = shear velocity, m/s;

k = Von Karman's constant, 0.4;

y = distance from the wall, m; and,

y_o = distance at which the velocity is zero, m.

The rough equation was used due to the roughness of the sand on the wall and sample mixture. To determine u(y), the velocity time series were first filtered by removing data points with correlation less than 40% and with signal to noise ratio (SNR) values less than 10 dB; if more than 15% of the time series for a particular u(y) were filtered out, the entire 1-mm bin was removed. After filtration the data were averaged for the entire 5-min run (Appendix B). The value of u* was then determined by fitting a line with a zero intercept to u(y) versus $\ln(y/y_o)$. Because y_o changed with every flow condition and soil type, the y_o value was adjusted until the best correlation of fit was obtained for each run. For some profiles, data points fell outside of the logarithmic profile in either the buffer layer or the outer layer. These points were not used in the calculation of τ_o. Velocity profiles which had four points or fewer remaining after data filtration were removed from analysis. The calculated erosion rate was divided by shear velocity to obtain a non-dimensional, normalized erosion rate, Er/u*, which accounted for differences in shear stress for each run. All 5-min. shear settings for each temperature could then be compared.

As the distribution of Er/u* was unknown, the bootstrap method was utilized to determine if the difference in means of Er/u* for two temperatures was significantly different from zero based on a one-tailed, lower 5% confidence interval (Haukoos and Lewis, 2005). Additionally, the Mann-Whitney nonparametric 2-sample test was also used to determine significant differences in median Er/u* values for different temperatures (Appendix C). Correlation between zeta potential and Er/u* for each soil and each average water temperature was determined using the Kendall and Spearman tests (Appendix C) (Dalgaard, 2008).

Chapter 4 Results

The observed erosional processes differed between the three clay types. While kaolinite samples eroded as small particles no larger than 1 mm in diameter, the vermiculite-dominated soil samples eroded as flakes approximately 1-5 mm in length. The montmorillonite samples typically had little particle erosion, but frequently experienced mass erosion when a 0.5-2 cm thick section of sample separated from the core. Erosion for all three soils was inconsistent—some samples eroded at a low shear stress, but did not erode under higher shear stresses.

Erosion Rate

In general there was little correlation between boundary shear stress and erosion rate for all clay types. As shown in Figure 4.1, there was a great deal of scatter in the data, but it is still clear that is in increase in erosion rate with increasing water temperature for kaolinite and vermiculite. The erosion rate of kaolinite ranged from 0.00-0.72, 0.35-1.20, and 0.48-1.47 cm/hr with mean erosion rates of 0.25, 0.80, and 0.98 cm/hr for water temperatures of 12, 20, and 27˚C, respectively. For vermiculite-dominated soil samples, the erosion rate varied from 0.00-0.58, 0.00-1.08, and 0.36-1.64 cm/hr with mean erosion rates of 0.15, 0.27, and 0.85 for water temperatures of 12, 20, and 27˚C, respectively. The erosion rate of montmorillonite samples ranged from 0.00-0.48, 0.00-0.48, and 0.00-0.43 cm/hr with mean erosion rates of 0.05, 0.10, and 0.07 for water temperatures of 12, 20, 27˚C, respectively. The montmorillonite erosion rates only reflect fluvial erosion and do not include mass erosion events. All results for erosion rate and flow conditions are listed in Appendix A.

During testing we found that the first flume setting (setting 1, Table 3.1) produced unusually high erosion rates when compared to the other settings; this was likely a result of the long wait time for the flow to become uniform causing a breakdown of the surface after sitting in water. Because of this, the first setting was removed from data analysis because the loss of soil was more likely due to breakdown of the surface strength with increasing moisture content rather than detachment caused by hydraulic stresses.

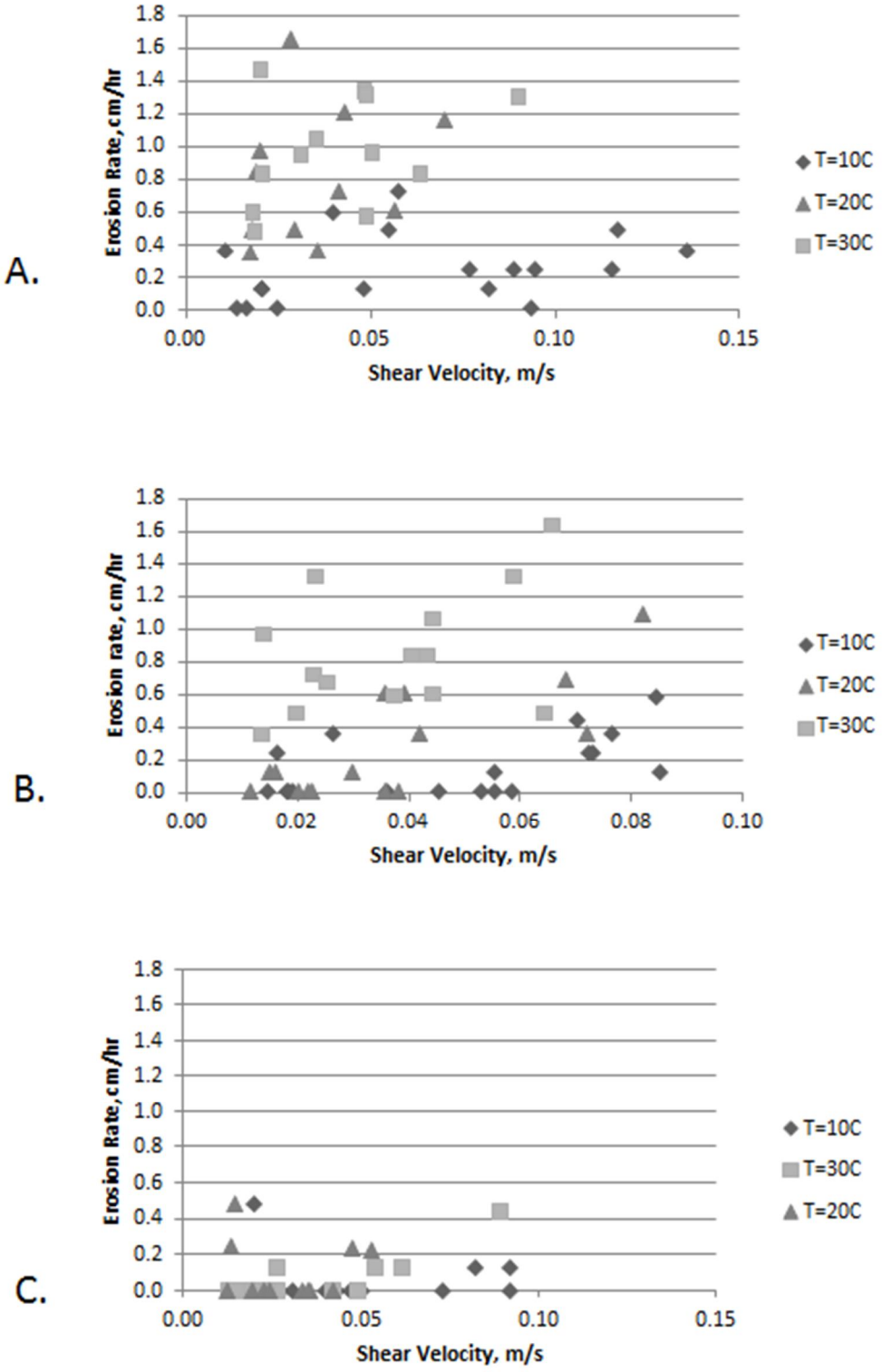

Figure 4.1 Erosion rate vs. shear velocity for each run of A. kaolinite mixture, B. vermiculite-dominated soil, and C. montmorillonite mixture at each average water temperature

A plot of cumulative erosion versus time for kaolinite at 12˚C is shown in Figure 4.2A; the full results, located in Appendix A, show a generally increasing erosion rate with increasing shear stress. Overall there was a consistent response for each of the three replicates. These plots also indicate that there was little influence of increasing moisture content over time since there were no notable changes in erosion rate when the second core was tested. Looking at the cumulative erosion plots in Appendix A, it is clear that the water temperature influenced erosion rate for kaolinite and vermiculite samples based on the increase in slopes with increasing temperature. Additionally, it can be seen that the slopes of the lines generally increase with increasing shear stress indicating there is some response in erosion rate to increasing the shear stress. On the plots for montmorillonite, the mass wasting events are clearly indicated by steep, near-vertical slopes (e.g. Figure 4.2B).

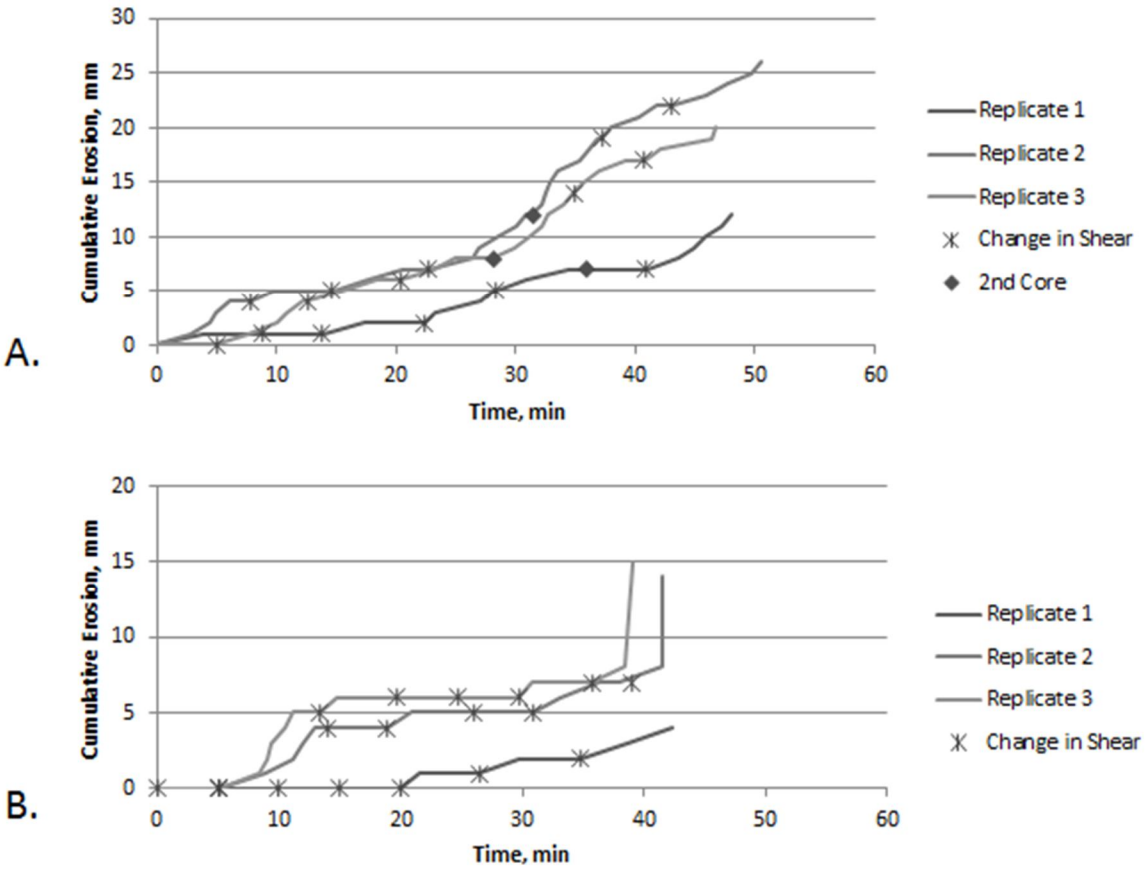

Figure 4.2 Cumulative erosion vs. time for A. kaolinite replicates, and B. montmorillonite replicates at 12˚C; An asterisk indicates a change in flume setting, and the diamonds indicate when the second core was started

To compare erosion rates independent of the applied shear stress the erosion rate, Er, was divided by shear velocity, u*. The variable Er/u* is a normalized, non-dimensional value of erosion which was used to compare all runs simultaneously while accounting for variation in shear velocity. The distribution of Er/u* for each soil based on water temperature is displayed in Figure 4.3. In general, the tests at 12˚C had the lowest variance in erosion rate for all clay types. Variability of erosion increased at increased water temperatures. The plots clearly show that the median erosion rate for vermiculite and kaolinite increased with water temperature.

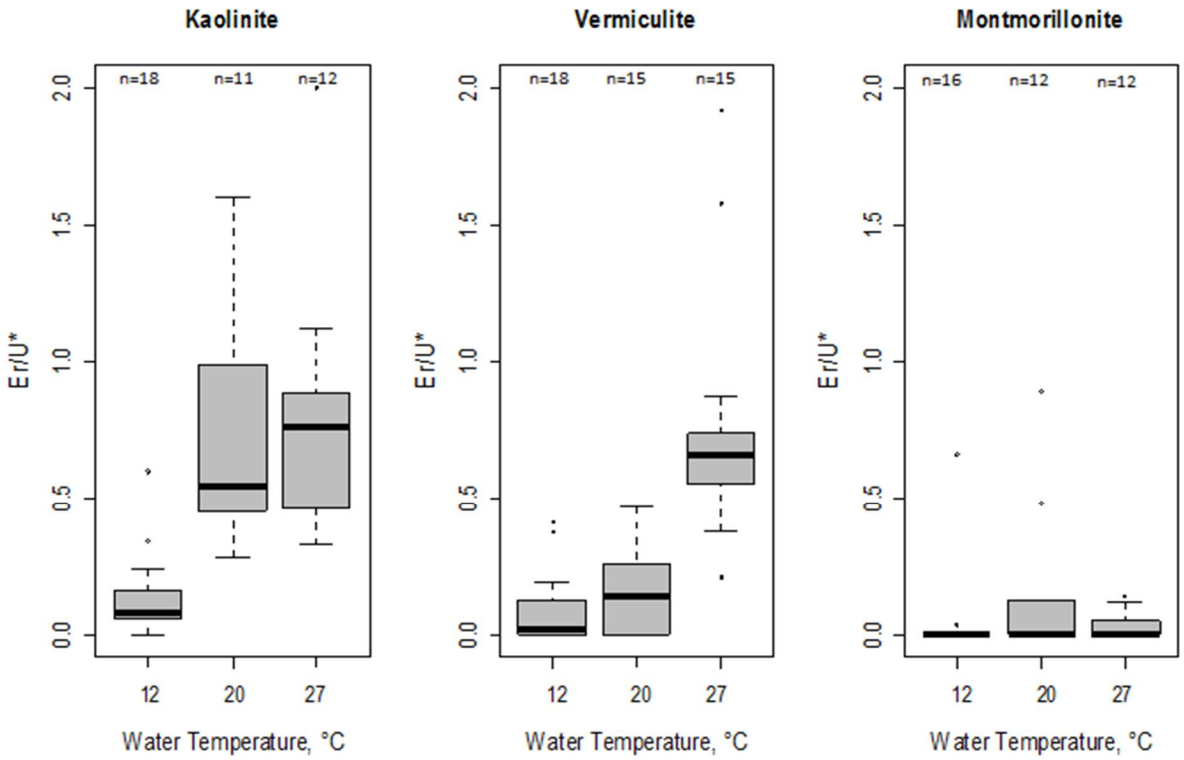

Figure 4.3 Distribution of erosion rate divided by shear shear velocity, Er/u*, at each average water temperature

Due to the unknown and unequal variance of the data, the bootstrap method was used to determine if the observed differences in mean values of Er/u* with water temperatures was significant. A significant difference was determined assuming a one-sided, lower confidence interval with 95% probability. The difference in samples show a statistically significant increase if the lower confidence bound is greater than zero. As seen in Table 4.1, there was a significant

increase in Er/u* for kaolinite when water temperature increased from 12 to 20˚C and for vermiculite-dominated soil samples when the water temperature increased from 20-27˚C. No significant increase in erosion rate occurred for montmorillonite with water temperature. In addition to the bootstrap method, a Mann-Whitney one-tailed, lower nonparametric test was conducted for each temperature change. As seen in Table 4.2, the results concur with findings from the bootstrap method. The mean erosion rate for kaolinite samples doubled when the temperature rose from 12-20˚C. Similarly, the average erosion rate for vermiculite-dominated soil more than tripled when the temperature increased from 20-27˚C. Fluvial erosion of montmorillonite was not significantly increased at higher water temperatures.

Table 4.1 Summary of bootstrap analysis for significant increase in mean erosion rate divided by shear velocity, Er/u*, for each temperature increase

Sample	Temperature change, ˚C	Sample number, n	Mean difference in Er/u*	Lower 95% confidence bound	Significant increase in Er/u*?
Kaolinite	20 to 27	18	0.07	-0.23	No
	12 to 27	11	0.66	0.46	Yes
	12 to 20	12	0.60	0.39	Yes
Vermiculite	20 to 27	16	0.58	0.41	Yes
	12 to 27	12	0.66	0.48	Yes
	12 to 20	12	0.08	-0.01	No
Montmorillonite	20 to 27	18	-0.11	-0.24	No
	12 to 27	15	-0.02	-0.10	No
	12 to 20	15	0.09	-0.04	No

Previous research has shown that total suspended solids (TSS) can influence erosion rate due to abrasion of the soil surface by suspended sediment (Oschwald, 1971). Therefore, TSS was sampled during the second replicate of each clay-temperature combination to test for TSS (Table 4.3). Although the flume water was cloudy at the time samples were taken, it is evident that the overall TSS levels were low during testing. There was likely little sand in the recirculated flow as it settled in the flume storage tank. The highest TSS corresponded to the montmorillonite samples at 20˚C which also had the greatest number of mass erosion events. The TSS samples

cannot be used as a secondary calculation of erosion rate as sediment settled in the storage tank during testing.

Table 4.2 Results from Mann-Whitney nonparametric t-test comparing erosion rate divided by shear velocity for each water temperature increase

Sample	Temperature change, ˚C	p-value	Significant increase in Er/u*?
Kaolinite	20 to 27	0.311	No
	12 to 27	< 0.001	Yes
	12 to 20	< 0.001	Yes
Vermiculite	20 to 27	< 0.001	Yes
	12 to 27	< 0.001	Yes
	12 to 20	0.095	No
Montmorillonite	20 to 27	0.700	No
	12 to 27	0.207	No
	12 to 20	0.157	No

Table 4.3 Total suspended sediments (TSS) of eroding water during testing

Sample	Water temperature, ˚C	TSS, mg/L
Source	N/A	2
Kaolinite	12	10
	20	17
	27	22
Vermiculite	12	19
	20	24
	27	49
Montmorillonite	12	23*
	20	59
	27	15

* Sample taken after 3rd replicate

Zeta Potential

Zeta potential was measured for each soil at each water temperature and compared to the mean Er/u* value (Figure 2.3). Generally, the zeta potential increased with decreasing temperature for all clay types, indicating a decrease in the double layer thickness at lower temperatures. Kaolinite samples had the strongest linear trend between Er/u* and zeta potential

based on the limited data collected in this study. To test for correlation, the Kendall and Spearman correlation test were conducted for each zeta potential—Er/u* pair (Table 4.4); however, due to the limit number of data points, the results were mostly inconclusive. While kaolinite and vermiculite dominated soil samples show perfect negative correlation, the p-value for each sample was too high for the correlation to be statistically significant. The results for montmorillonite samples showed no significant correlation with either test.

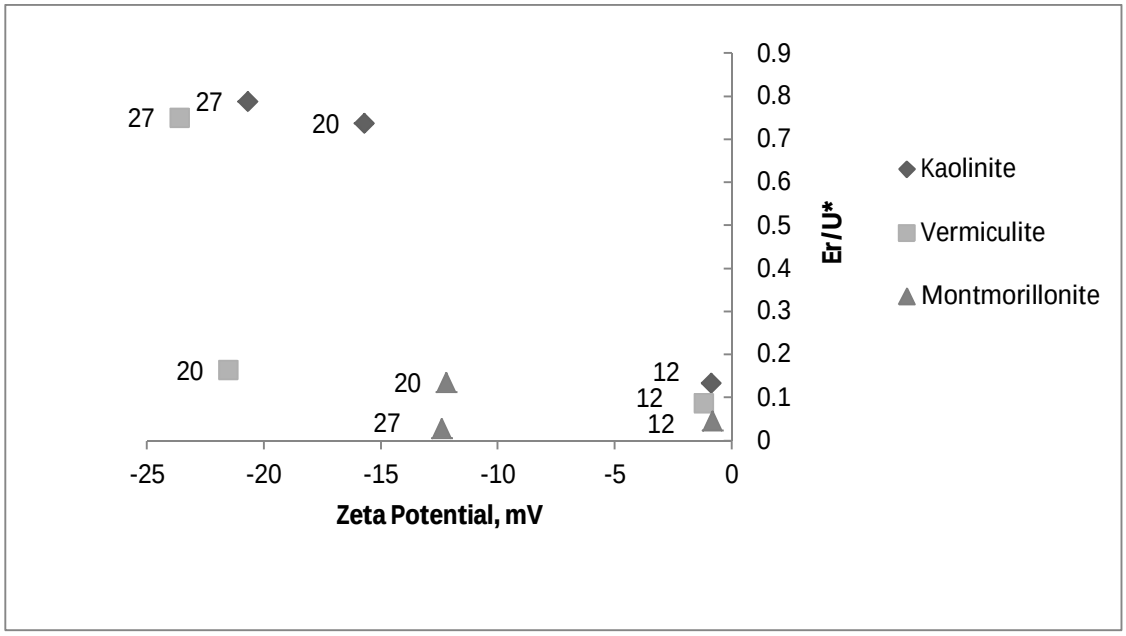

Figure 4.4 Average values of erosion rate divided by shear velocity, Er/u*, compared to zeta potential; water temperature, ˚C, is labeled for each point

Table 4.4 Summary of nonparametric tests for correlation between zeta potential and erosion rate divided by shear velocity, Er/u*

	Kendall's method		Spearman's method	
Sample	**p-value**	**Kendall's τ**	**p-value**	**Spearman's ρ**
Kaolinite	0.333	-1	0.333	-1
Vermiculite	0.333	-1	0.333	-1
Montmorillonite	1	0.333	1	0.5

Chapter 5 Discussion

Temperature Effect on Erosion Rate

A significant increase in erosion rate with increase in water temperature was observed for kaolinite and vermiculite-dominated soil samples. Kaolinite erosion increased by an average of 206% when water temperature changed from 12 to 20˚C; however, there was no significant change in erosion from 20 to 27˚C. The vermiculite-dominated soil samples showed no statistically significant change in erosion from 12 to 20˚C, but erosion increased by an average of 356% when the temperature increased from 20 to 27˚C.

While there was not a significant change in erosion rate for each temperature increase, the median values of Er/u* did increase for kaolinite and vermiculite samples for each temperature increase, and overall the erosion rate was significantly increased between 12 and 27˚C. When comparing the erosion rate for vermiculite between 12-20˚C, the p-value of the Mann-Whitney test was 0.095, which is still low, especially when one considers the small sample size. Additionally, as the temperature increased, the variance of Er/u* also increased for both soils (Figure 4.3). As seen in Figure 4.3, the variance in Er/u* was greatest at 20˚C for all three clays. Increase in the median value of Er/u* shows erosion was increasing with increasing temperature, but the variability of the data and the small sample size likely decreased the statistical significance of this increase. The erosion rate of kaolinite samples were by far the most variable of the three clay types; this is likely due to the less 'natural' composition of kaolinite samples as compared to the vermiculite.

High variability in erosion rates is not uncommon. Raudkivi and Hutchison (1974) observed erosion rates which doubled and tripled in value between four replicates of kaolinite bed erosion. However, many researchers only tested one sample under each experimental condition and did not statistically fit a trend line to data, which means the goodness of fit was also not quantified (Christensen and Das, 1973; Kelly and Gularte, 1981; Zreik et al., 1998). Based on the results of this study, and previously observed results, it is clear that cohesive soil erosion is quite variable. Conclusions drawn from this study are more powerful than studies which only tested one sample; however, it would still be beneficial to increase the number of replicates in future studies.

There was no correlation between erosion rate and water temperature for the montmorillonite samples. This observation is supported by previous research. Raudkivi and Hutchison (1974) tested for temperature effects on the erosion of kaolinite samples of different D_{50} grain size (<1, 2-5, and 5-8 μm). The authors found that the smaller grain size had greater surface-to-surface, or platey bonding, which was stronger than the bonds of the larger, more granular particles with less-oriented bonding. The smallest grain size was least affected by temperature changes in the water, which led the authors to conclude that the effect of water temperature increases became less significant as the cohesive, or inter-particle bond strength, increased. Additionally, Zreik et al. (1998) found that water temperature mainly influenced the first 0.5 mm of Boston Blue Clay, beyond which the soil structure and sample age were dominating factors influencing erosion rates. These conclusions support the trends of montmorillonite erosion observed in this study. The montmorillonite samples were not influenced by temperature, and erosion was primarily due to mass failure of the sample. It is believed that the high cohesion of the montmorillonite limited surface erosion due to fluvial stresses; however, mass erosion occurred once the structural strength of the sample was surpassed as the sample weight and moisture content increased following wetting. This finding is supported by observations at the Virginia Tech StREAM laboratory, where bank retreat of the lower, montmorillonite-dominated bank layer is primarily due to mass wasting. From these results it is clear that the effect of temperature on erosion rate varied with mineralogy.

To the best of the authors' knowledge, this study is the first flume study of cohesive soil erosion which has placed the sample in the flume wall, rather than the channel bed. The vertical orientation allows processes of both fluvial and mechanical erosion to occur; only fluvial erosion is possible for samples placed in the channel bed. As noted by the differences in erosion processes between the different clay samples, the ability to discriminate between mass wasting and fluvial erosion is important when studying cohesive soils. Additionally, fluvial erosion differs between channel beds and streambanks. For fluvial erosion to occur in a channel bed, both detachment and entrainment are needed to remove soil particles from the surface. Conversely, particles from the streambank are removed from the soil once detachment occurs, as gravity or fluid flow moves the particle away from the surface. Therefore, erosion from a streambank requires less energy and can theoretically occur at lower shear stresses, and regardless of stream transport capacity.

Previous research has noted a rapid increase in erosion with increasing shear stress (Christensen and Das, 1973; Zreik et al., 1998). For this study, no critical shear stress at which erosion began or rapidly increased was observed; in fact, there was little correlation between shear stress and erosion rate. Study results suggest that shear stress is not a good indicator of erosion rates for cohesive soils.

Zeta Potential

In general, the zeta potential decreased (became more negative) with increasing temperature, indicating an increase in the double layer thickness and greater repulsion between soil particles (Baumgarten et al., 2012). Based on this data, it can be inferred that clay particles would be more easily eroded at a lower zeta potential when there is greater repulsion. Kaolinite samples show the best positive correlation between zeta potential and erosion rates. However, one would expect the erosion rate of the vermiculite soil sample to be higher at the lower zeta potential at 20˚C. While the dilute vermiculite sample was first settled in an attempt to sample only the clay fraction, it is possible that iron oxides in the sample interfered with the readings. One would also expect montmorillonite to have a much lower zeta potential at warmer temperatures. The inconsistency of the zeta potential measurement of the montmorillonite sample at 20 and 27˚C can be explained by carbonates on the clay surfaces which masked surface potential. Also, as montmorillonite erosion was dominated by mass erosion, it is not expected to see the erosion rate correlate with zeta potential.

Raudkivi and Hutchison (1974) also theorized that erosion rate could be correlated with zeta potential. Their study determined the zeta potential for two different grain sizes of kaolinite (< 1μm, and 2-5 μm) at different salinities (0, 0.005, and 0.010 mol/l $NaNO_3$). Unfortunately, the authors only measured zeta potential at one unspecified temperature, so the results cannot be compared to this study. However, their results indicated that the maximum erosion resistance coincided with the lowest zeta potential for solutions at 0.005 and 0.01 M $NaNO_3$.

Ramachandran and Somasundaran (1986) also studied the effect of temperature on the zeta potential of kaolinite at 25 and 75˚C. The authors observed a decrease in zeta potential with increasing temperature over this range; however, the authors also observed a hysteresis effect as the zeta potential did not return to the original value when the temperature was returned to 25˚C following heating. The zeta potential values for this study were first taken at 27˚C then at

temperatures of 20, and 12˚C. It is possible that the zeta potential values were affected by a hysteresis effect, but this unlikely because the temperatures tested in this study was much lower and the range of temperature was much smaller than the range in Ramachandran and Somasundaran (1986).

Rodriguez and Araujo (2006) and Ramachandran and Somasundaran (1986) both observed an effect of solution pH on the zeta potential of kaolinite samples. At an acidic pH the zeta potential was generally positive, and at alkaline pH the zeta potential was negative, due changes in surface speciation at different pH values. However, the zeta potential decreased with increasing temperature for all pH values. For this study, the clays were suspended in DI water, and the pH was not adjusted.

As pH, salinity, and temperature have been shown to affect both cohesive soil erodibility and zeta potential, the use of zeta potential as an indicator of erodibility for a given environmental condition should be further explored (Grabowski et al., 2011; Ramachandran and Somasundaran, 1986; Raudkivi and Hutchison, 1974). For this research, the zeta potential measured at the temperature of the eroding water showed some correlation to erosion rates of kaolinite and vermiculite samples; however, the results were not conclusive due to the limited sample size.

Variability in the Data

While variability is inherent to the study of cohesive soil erosion, some variability can be attributed to the methods of the experimental design and data collection. The most notable sources of error of this study were likely due to the sample making process and the lack of precision available when changing flume settings. Each soil core was made individually by hand-mixing the clay, sand, water mixture, and using a bulk density hammer to compact the sample. While the error in the amount of clay and sand added to the mixture was within 0.05 g, small amounts of the mixture were lost by sticking to the bowl walls and while transferring the mixture into the soil core. Additional variability in the cores arose during the compaction process; each core was not compressed under a precise force, but rather a relatively uniform force delivered by the slide hammer. A final source of variability in samples was the time between sample creation and testing. The cores used for each clay-temperature combination were created in a batch and were tested within hours of each other. However, the time between

core creation and testing for different batches and different clay-temperature combinations ranged from 4-9 days. Zreik et al. (1998) tested the erosion rate of samples of Boston Blue Clay settled from suspension and consolidated for a period of 1.8-18.9 days. The authors observed an increase in erosion resistance of the soil with increased sample age.

Variation in boundary shear stress can be partially attributed to the lack of precision available when adjusting the tailgate height and slope of the flume channel. Both of these settings are manually adjusted and measured. It is possible that the tailgate height varied ± 2 mm during testing. The error in the bed slope is unknown as the slope reading is made with a adjustable bubble level. However, the flow rate of the water is precisely controlled based on pump frequency which can be set to $1/10^{th}$ Hz precision. Further variation in the boundary shear stress could be caused by secondary currents in the channel. While flume settings were chosen which displayed uniform flow through the test section based on velocity profile measurements down the center of the channel and near the wall, there may be hydraulic forces interacting with the soil surface which were not detected.

Broader Impacts

The findings of this research are particularly significant in light of growing human populations and climate change. Summer storm runoff from urbanized areas transports a large volume of heated water into streams. Not only does the increased flow rate increase streambank erosion, it has now been shown that the warmer water temperatures decrease erosion resistance of the banks. Furthermore, as stream temperatures rise due to climate change, it is likely that there will be an increase in erosion in streams with cohesive banks even in rural areas. The results of this study also have implications for watershed modeling and management. When modeling annual stream erosion, the difference in water temperature during summer and winter months could be affecting erosion rates and sediment yield, therefore critical shear stress and erodibility should be modeled as a function of temperature, rather than considered constant. Watershed management practices should also aim at decreasing elevated water temperatures (i.e. stormwater runoff, or industrial wastewater) before the water enters the receiving waters to help reduce erosion of streambanks. Additionally, with further research, measurement of zeta potential could be a relatively economical method to determine the erodibility of cohesive soils.

Chapter 6 Conclusions

This research determined erosion rates of cohesive soils with kaolinite and vermiculite mineralogy significantly increase with increasing stream temperature. Erosion of vermiculite-dominated soil samples more than tripled with a 15˚C increase in water temperature. Research results also showed that the effect of water temperature on erosion rates varied with clay mineralogy and soil structure. The erosion of montmorillonite, a clay with high cohesion, was not influenced by temperature; rather, the loss of structural strength of the sample dominated erosion events as indicated by many occurrences of mass erosion during testing. This result indicated that water temperature effects became less significant as inter-particle bond strength increases. Additionally, the mode of montmorillonite erosion demonstrated that the vertical orientation of the sample in this study proved advantageous as the erosion processes (i.e. fluvial versus mechanical) could be discriminated. The variability in erosion rates of all clay types showed that multiple replications are necessary when studying cohesive soil erodibility. Although conclusive results cannot be made at this time due to limited sample size (n=3), zeta potential values show some correlation with erosion rate.

Research should continue to explore the influence of water temperature on the erosion of cohesive soils to better understand the interaction between water temperature and different clay properties. It is recommended that samples be placed in a vertical orientation, and that multiple replicates are conducted for each treatment. The possibility of using zeta potential as an indicator of erodibility should be further explored, especially under different pH and salinity conditions. Watershed modeling and management should account for the influence of water temperature on cohesive streambank erosion, especially with regards to urbanization and climate change.

References

Backlund, P., A. Janetos, D. S. Schimel, J. Hatfield, M. G. Ryan, S. R. Archer, and D. Lettenmaier. 2008. The effects of climate change on agriculture, land resources, water resources, and biodiversity in the United States. 362. USCCSPatSoGC Research, ed. Washington, DC, USA.

Baumgarten, W., T. Neugebauer, E. Fuchs, and R. Horn. 2012. Structural stability of marshland soils of the riparian zone of the Tidal Elbe River. *Soil & Tillage Research* 125:80-88.

Brady, N. C., and R. R. Weil. 2008. *The Nature and Properties of Soils*. 14 ed. Pearson Prentice Hall, Upper Saddle River, NJ.

Christensen, R. W., and B. M. Das. 1973. Hydraulis erosion of remolded cohesive soils. *Soil Erosion: Causes and Mechanisms, Prevention and Control, Special Report 135*:8-19.

Dalgaard, P. 2008. *Introductory Statistics with R*. 2 ed. Springer, New York, NY.

Docker, B. B., and T. C. T. Hubble. 2008. Quantifying root-reinforcement of river bank soils by four Australian tree species. *Geomorphology* 100(3-4):401-418.

Edwards, A. P., and J. M. Bremner. 1967. Microaggregates in soils. *Journal of Soil Science* 18(1):64-73.

Gaskin, S. J., J. Pieterse, A. Al Shafie, and S. Lepage. 2003. Erosion of undisturbed clay samples from the banks of the St. Lawrence River. *Canadian Journal of Civil Engineering* 30(3):585-595.

Grabowski, R. C., I. G. Droppo, and G. Wharton. 2011. Erodibility of cohesive sediment: The importance of sediment properties. *Earth-Science Reviews* 105(3-4):101-120.

Grissinger, E. H. 1966. Resistance of selected clay systems to erosion by water. *Water Resources Research* 2(1):131-138.

Harris, W. G., S. S. Iyengar, L. W. Zelazny, J. C. Parker, D. A. Lietzke, and W. J. Edmonds. 1980. Mineralogy of a chronosequence formed in New River alluvium. *Soil Science Society of America Journal* 44(4):862-868.

Haukoos, J. S., and R. J. Lewis. 2005. Advanced statistics: Bootstrapping confidence intervals for statistics with "difficult" distributions. *Academic Emergency Medicine* 12(4):360-365.

Kamphuis, J. W., and K. R. Hall. 1983. Cohesive material erosion by unidirectional current. *Journal of Hydraulic Engineering-Asce* 109(1):49-61.

Kelly, W. E., and R. C. Gularte. 1981. Erosion resistance of cohesive soils. *Journal of the Hydraulics Division-Asce* 107(10):1211-1223.

Kozarek, J. L. 2011. Channel morphology and riparian vegetation influences on fluvial aquatic habitat. Virginia Polyechnic Institute and State University, Biological Systems Engineering, Blacksburg, VA

Kundu, P. K. 1990. *Fluid Mechanics*. Academic Press, San Diego, CA.

Laird, D. A. 2006. Influence of layer charge on swelling of smectites. *Applied Clay Science* 34(1-4):74-87.

LeBlanc, R. T., R. D. Brown, and J. E. FitzGibbon. 1997. Modeling the effects of land use change on the water temperature in unregulated urban streams. *Journal of Environmental Management* 49(4):445-469.

Li, H., S. Q. Wei, C. L. Qing, and J. S. Yang. 2003. Discussion on the position of the shear plane. *Journal of Colloid and Interface Science* 258(1):40-44.

McBride, M. B. 1994. *Environmental Chemistry of Soils*. Oxford University Press, New York, New York.

Mohseni, O., T. R. Erickson, and H. G. Stefan. 1999. Sensitivity of stream temperatures in the United States to air temperatures projected under a global warming scenario. *Water Resources Research* 35(12):3723-3733.

Moody, J. A., J. D. Smith, and B. W. Ragan. 2005. Critical shear stress for erosion of cohesive soils subjected to temperatures typical of wildfires. *Journal of Geophysical Research-Earth Surface* 110.

Nelson, K. C., and M. A. Palmer. 2007. Stream temperature surges under urbanization and climate change: Data, models, and responses. *Journal of the American Water Resources Association* 43(2):440-452.

Oschwald, W. R. 1971. Sediment-water interactions. *Journal of Environmental Quality* 1(4):360-366.

Parchure, T. M., and A. J. Mehta. 1985. Erosion of soft cohesive sediment deposits. *Journal of Hydraulic Engineering-ASCE* 111(10):1308-1326.

Partheniades, E. 1965. Erosion and deposition of cohesive soils. *Journal of the Hydraulics Division-ASCE* 91(1):105-139.

Ramachandran, R., and P. Somasundaran. 1986. Effect of temperature on the interfacial properties of silicates. *Colloids and Surfaces* 21:355-369.

Raudkivi, A. J., and D. L. Hutchison. 1974. Erosion of kaolinite clay by flowing water. *Proceedings of the Royal Society of London. Series A, Mathematical and Physical Sciences* 337(1611):537-554.

Rodriguez, K., and M. Araujo. 2006. Temperature and pressure effects on zeta potential values of reservoir minerals. *Journal of Colloid and Interface Science* 300(2):788-794.

Shang, J. Q., K. Y. Lo, and R. M. Quigley. 1994. Quantitative-determination of potential distribution in Stern-Gouy double-layer model. *Canadian Geotechnical Journal* 31(5):624-636.

Simon, A., A. Curini, S. E. Darby, and E. J. Langendoen. 2000. Bank and near-bank processes in an incised channel. *Geomorphology* 35(3-4):193-217.

Stefan, H. G., and B. A. Sinokrot. 1993. Projected global climate-change impact on water temperatures in 5 north central United-States streams. *Climatic Change* 24(4):353-381.

Taylor, B. D., and V. A. Vanoni. 1972. Temperature effects in low transport, flat bed flows. *Journal of the Hydraulics Division-ASCE* 98(8):1427-1445.

Thorne, C. R., C. Alonso, R. Bettess, D. Borah, S. Darby, P. Diplas, P. Julien, D. Knight, L. G. Li, J. Pizzuto, M. Quick, A. Simon, M. Stevens, S. Wang, C. Watson, and B. M. ASCE Task Comm Hydraulics, M. o. d. e. l. i. n. g. 1998. River width adjustment. I: Processes and mechanisms. *Journal of Hydraulic Engineering-ASCE* 124(9):881-902.

Trimble, S. W. 2009. Fluvial processes, morphology and sediment budgets in the Coon Creek Basin, WI, USA, 1975-1993. *Geomorphology* 108(1-2):8-23.

USDI. 1963. Canal erosion and tractive force study analysis of data from a boundary shear flume. 34. B. o. Reclamation, ed. Denver, CO: USDI.

USEPA. 2008. Environmental impact and benefits assessment for proposed effluent guidelines and standards for the construction and developement category. USEPA, Washington, DC: USEPA.

USEPA. 2010. National summary of impaired waters and TMDL information. Washington, DC: USEPA.

USGS. 2003. A summary report of sediment processes in Chesapeake Bay and watershed. 122. W.-R. Investigation, New Cumberland, PA: USGS.

Van Buren, M. A., W. E. Watt, J. Marsalek, and B. C. Anderson. 2000. Thermal enhancement of stormwater runoff by paved surfaces. *Water Research* 34(4):1359-1371.

Zhu, Y. H., J. Y. Lu, H. Z. Liao, J. S. Wang, B. L. Fan, and S. M. Yao. 2008. Research on cohesive sediment erosion by flow: An overview. *Science in China Series E-Technological Sciences* 51(11):2001-2012.

Zreik, D. A., B. G. Krishnappan, J. T. Germaine, O. S. Madsen, and C. C. Ladd. 1998. Erosional and mechanical strengths of deposited cohesive sediments. *Journal of Hydraulic Engineering-Asce* 124(11):1076-1085.

Appendix A General Results

Table A.1 Erosion rate and flow data for kaolinite samples at an average water temperature of 12˚C

Replicate	Flume Setting	Avg water temp, ˚C	Best y_o, mm	Correlation to rough equation	Shear Velocity, u*, m/s	Boundary shear stress, τ_o, Pa	Erosion rate, cm/hr	Er/u*
1	1	10.45	0.01	0.998	0.010	0.11	0.00	0.00
	2	10.57	0.0001	0.9939	0.011	0.13	0.00	0.00
	3	10.85	0.001	0.9882	0.021	0.47	0.00	0.00
	4	10.92	0.03	0.9964	0.048	2.46	0.24	0.14
	5	11.20	0.006	0.9901	0.040	1.69	0.12	0.08
	6	11.57	0.08	0.9946	0.095	9.45	0.00	0.00
	7	11.95	0.15	0.9953	0.116	14.14	4.14	0.11
2	1	12.29	0.03	0.9976	0.012	0.15	0.36	0.84
	2	12.32	0.01	0.9759	0.014	0.21	0.00	0.00
	3	12.47	0.001	0.9904	0.021	0.45	0.12	0.16
	4	12.64	0.09	0.9912	0.055	3.21	0.48	0.24
	5	12.88	0.1	0.9978	0.058	3.55	0.72	0.34
	6	13.17	0.09	0.999	0.089	8.39	0.24	0.07
	7	13.53	0.3	0.9991	0.136	19.44	0.36	0.07
3	1	11.78	0.009	0.9973	0.010	0.11	0.00	0.00
	2	11.79	0.008	0.9955	0.017	0.30	0.36	0.60
	3	12.09	0.01	0.9988	0.025	0.68	0.12	0.13
	4	12.13	0.19	0.9985	0.077	6.30	0.12	0.04
	5	12.39	0.15	0.999	0.083	7.19	0.59	0.20
	6	12.71	0.1	0.9994	0.094	9.23	0.24	0.07
	7	13.01	0.15	0.9998	0.117	14.48	0.24	0.06

Table A.2 Erosion rate and flow data for kaolinite samples at an average water temperature of 20˚C

Replicate	Flume Setting	Avg water temp, ˚C	Best y_o, mm	Correlation to rough equation	Shear Velocity, u*, m/s	Boundary shear stress, τ_o, Pa	Erosion rate, cm/hr	Er/u*
1	1	19.29	0.028	0.9944	0.011	0.14	0.35	0.85
	2	19.10	0.023	0.9974	0.018	0.34	0.35	0.54
	3	19.10	0.00034	0.9858	0.018	0.35	0.48	0.73
	4	19.08	0.02	0.9982	0.042	1.82	0.72	0.48
	5	N/A*						
	6	N/A*						
	7	N/A*						
2	1	19.10	0.08	0.9942	0.014	0.20	1.20	2.42
	2	19.10	0.04	0.9903	0.019	0.39	0.84	1.21
	3	19.20	0.025	0.9989	0.030	0.93	0.48	0.45
	4	19.14	0.008	0.9971	0.036	1.37	0.36	0.28
	5	19.36	0.05	0.9968	0.057	3.40	0.60	0.29
	6	N/A*						
	7	N/A*						
3	1	19.44	0.09	0.9973	0.014	0.21	1.32	2.61
	2	19.44	0.06	0.9956	0.021	0.44	0.96	1.30
	3	19.58	0.02	0.9987	0.029	0.87	1.65	1.60
	4	19.59	0.03	0.9995	0.043	1.96	1.20	0.77
	5	19.70	0.16	0.9942	0070	5.20	1.15	0.45
	6	N/A*						
	7	N/A*						

* Flume setting not reached during testing

Table A.3 Erosion rate and flow data for kaolinite samples at an average water temperature of 27˚C

Replicate	Flume Setting	Avg water temp, ˚C	Best y_o, mm	Correlation to rough equation	Shear Velocity, u*, m/s	Boundary shear stress, τ_o, Pa	Erosion rate, cm/hr	Er/u*
1	1	28.35	0.09	0.9931	0.014	0.21	1.22	2.39
	2	28.16	0.07	0.9983	0.021	0.46	0.84	1.12
	3	28.13	0.07	0.9988	0.035	1.31	1.05	0.82
	4	27.84	0.05	0.9997	0.049	2.49	1.35	0.77
	5	N/A*						
	6	N/A*						
	7	N/A*						
2	1	27.83	0.026	0.9987	0.011	0.14	0.60	0.145
	2	27.75	0.033	0.9979	0.018	0.35	0.60	0.92
	3	27.56	0.0015	0.9890	0.020	0.44	1.47	2.00
	4	27.41	0.05	0.9973	0.049	2.52	0.58	0.33
	5	27.46	0.1	0.9870	0.064	4.22	.84	0.37
	6	27.35	0.09	0.9870	0.090	8.56	1.31	0.40
	7	N/A*						
3	1	27.43	0.04	0.9883	0.013	0.17	1.20	2.64
	2	27.27	0.04	0.9918	0.019	0.36	0.48	0.72
	3	27.25	0.05	0.9880	0.031	1.03	0.95	0.84
	4	26.99	0.04	0.9985	0.049	2.54	1.32	0.74
	5	27.19	0.03	0.9983	0.051	2.70	0.96	0.52
	6	N/A*						
	7	N/A*						

* Flume setting not reached during testing

Table A.4 Erosion rate and flow data for vermiculite-dominated soil samples at an average water temperature of 12˚C

Replicate	Flume Setting	Avg water temp, ˚C	Best y_o, mm	Correlation to rough equation	Shear Velocity, u*, m/s	Boundary shear stress, τ_o, Pa	Erosion rate, cm/hr	Er/u*
1	1	10.74	0.020	0.9935	0.013	0.16	0.24	0.53
	2	10.92	0.018	0.9922	0.018	0.34	0.00	0.00
	3	11.07	0.013	0.9992	0.026	0.72	0.36	0.38
	4	11.16	0.09	0.9828	0.055	3.23	0.12	0.06
	5	11.34	0.08	0.9854	0.055	3.23	0.00	0.00
	6	11.78	0.05	0.9946	0.085	7.62	0.12	0.04
	7	12.17	0.005	0.9994	0.070	5.19	0.43	0.17
2	1	11.03	0.023	0.9924	0.012	0.16	0.36	0.81
	2	11.11	0.009	0.9877	0.018	0.35	0.00	0.00
	3	11.29	0.0002	0.9982	0.016	0.28	0.24	0.41
	4	11.43	0.021	0.9855	0.045	2.16	0.00	0.00
	5	11.67	0.0014	0.9883	0.036	1.37	0.00	0.00
	6	12.04	0.015	0.9966	0.073	5.57	0.24	0.09
	7	12.44	0.02	0.9960	0.084	7.47	0.58	0.19
3	1	11.45	0.015	0.9950	0.012	0.14	0.36	0.85
	2	11.57	0.003	0.9940	0.014	0.22	0.00	0.00
	3	11.75	0.001	0.9915	0.019	0.39	0.00	0.00
	4	11.78	0.14	0.9857	0.058	3.59	0.00	0.00
	5	12.02	0.045	0.9912	0.053	2.96	0.00	0.00
	6	12.26	0.021	0.9974	0.076	6.12	0.36	0.13
	7	12.58	0.008	0.9993	0.072	5.51	0.24	0.09

Table A.5 Erosion rate and flow data for vermiculite-dominated soil samples at an average water temperature of 20˚C

Replicate	Flume Setting	Avg water temp, ˚C	Best y_o, mm	Correlation to rough equation	Shear Velocity, u*, m/s	Boundary shear stress, τ_o, Pa	Erosion rate, cm/hr	Er/u*
1	1	20.12	0.02	0.9939	0.011	0.13	0.00	0.00
	2	20.12	0.0005	0.9840	0.012	0.14	0.00	0.00
	3	20.16	0.002	0.9964	0.022	0.49	0.00	0.00
	4	20.12	0.007	0.9872	0.036	1.34	0.00	0.00
	5	20.26	0.003	0.9978	0.038	1.53	0.00	0.00
	6	20.54	0.01	0.9961	0.068	4.88	0.69	0.28
	7	N/A+						
2	1	20.82	0.015	0.9974	0.011	0.12	0.00	0.00
	2	20.82	0.007	0.9937	0.015	0.24	0.12	0.22
	3	20.83	0.003	0.9944	0.022	0.53	0.00	0.00
	4	20.82	0.01	0.9915	0.039	1.61	0.60	0.42
	5	20.97	0.01	0.9981	0.042	1.83	0.36	0.24
	6	21.22	0.02	0.9931	0.072	5.45	0.35	0.14
	7	N/A+						
3	1	21.51	0.001	0.9867	0.008	0.06	0.00	0.00
	2	21.37	0.01	0.9965	0.016	0.26	0.12	0.21
	3	21.50	0.0008	0.9816	0.020	0.42	0.00	0.00
	4	21.50	0.001	0.9804	0.030	0.92	0.12	0.11
	5	21.59	0.003	0.9870	0.036	1.34	0.60	0.47
	6	21.81	0.028	0.9913	0.082	7.05	1.08	0.37
	7	N/A+						

+ Less than four data points remained in velocity profile after filtration; run removed from further analysis

Table A.6 Erosion rate and flow data for vermiculite-dominated soil samples at an average water temperature of 27˚C

Replicate	Flume Setting	Avg water temp, ˚C	Best y_o, mm	Correlation to rough equation	Shear Velocity, u*, m/s	Boundary shear stress, τ_o, Pa	Erosion rate, cm/hr	Er/u*
1	1	N/A±						
	2	27.99	0.04	0.9992	0.020	0.40	0.48	0.68
	3	27.83	0.007	0.9969	0.023	0.57	1.32	1.58
	4	27.77	0.018	0.9887	0.044	2.04	0.60	0.38
	5	27.79	0.005	0.9938	0.041	1.79	0.84	0.56
	6	N/A*						
	7	N/A*						
2	1	27.60	0.004	0.9993	0.009	0.09	0.96	2.94
	2	27.57	0.003	0.9954	0.013	0.19	0.36	0.74
	3	27.56	0.003	0.9995	0.023	0.56	0.72	0.87
	4	27.37	0.02	0.9905	0.044	2.07	1.06	0.66
	5	27.36	0.007	0.9901	0.041	1.72	0.84	0.58
	6	27.47	0.008	0.9950	0.065	4.35	0.48	0.21
	7	27.50	0.003	0.9995	0.066	4.50	1.64	0.69
3	1	27.43	0.005	0.9984	0.010	0.09	0.84	2.45
	2	27.43	0.004	0.9974	0.014	0.20	0.96	1.92
	3	27.41	0.007	0.9989	0.025	0.66	0.67	0.74
	4	27.21	0.02	0.9931	0.043	1.95	0.84	0.54
	5	27.32	0.002	0.9923	0.037	1.46	0.59	0.44
	6	27.50	0.004	0.9977	0.059	3.61	1.32	0.62
	7	N/A*						

± Velocity data was not recorded

* Flume setting was not reached during testing

Table A.7 Erosion rate and flow data for montmorillonite samples at an average water temperature of 12˚C

Replicate	Flume Setting	Avg water temp, ˚C	Best y_o, mm	Correlation to rough equation	Shear Velocity, u*, m/s	Boundary shear stress, τ_o, Pa	Erosion rate, cm/hr	Er/u*
1	1	N/A±						
	2	11.08	0.005	0.9877	0.015	0.24	0.00	0.00
	3	11.22	0.01	0.9933	0.027	0.76	0.00	0.00
	4	11.32	0.02	0.9920	0.043	1.98	0.00	0.00
	5	11.63	0.0005	0.9913	0031	1.01	0.00	0.00
	6	12.03	0.07	0.9978	0.092	8.88	0.00	0.00
	7	12.45	0.03	0.9959	0.092	8.88	0.12	0.04
2	1	11.61	0.008	0.9715	0.011	0.12	0.00	0.00
	2	11.75	0.012	0.9973	0.016	0.28	0.00	0.00
	3	11.91	0.009	0.9963	0.027	0.79	0.00	0.00
	4	12.00	0.03	0.9834	0.048	2.39	0.00	0.00
	5	12.21	0.004	0.9910	0.040	1.71	0.00	0.00
	6	12.56	0.04	0.9984	0.083	7.16	0.12	0.04
	7	N/A¥						
3	1	11.77	0.003	0.9803	0.009	0.09	0.00	0.00
	2	11.96	0.03	0.9961	0.020	0.42	0.48	0.66
	3	12.11	0.002	0.9918	0.021	0.44	0.00	0.00
	4	12.15	0.05	0.9786	0.050	2.66	0.00	0.00
	5	12.39	0.015	0.9922	0.047	2.33	0.00	0.00
	6	12.68	0.015	0.9984	0.073	5.62	0.00	0.00
	7	N/A¥+						

± Velocity data was not recorded

¥ Only mass erosion occurred; run removed from analysis

+ Less than four data points remained in velocity profile after filtration; run removed from analysis

Table A.8 Erosion rate and flow data for montmorillonite samples at an average water temperature of 20˚C

Replicate	Flume Setting	Avg water temp, ˚C	Best y_o, mm	Correlation to rough equation	Shear Velocity, u*, m/s	Boundary shear stress, τ_o, Pa	Erosion rate, cm/hr	Er/u*
1	1	19.96	0.0005	0.9968	0.007	0.05	0.00	0.00
	2	19.98	0.006	0.9993	0.015	0.23	0.48	0.89
	3	20.06	0.0005	0.9988	0.019	0.39	0.00	0.00
	4	20.22	0.007	0.9951	0.048	2.39	0.23	0.13
	5	N/A¥						
	6	20.56	0.002	0.9954	0.053	2.99	0.23	0.12
	7	N/A¥+						
2	1	20.12	0.0004	0.9967	0.007	0.05	0.00	0.00
	2	20.12	0.001	0.9950	0.012	0.16	0.00	0.00
	3	20.26	0.004	0.9949	0.023	0.55	0.00	0.00
	4	20.26	0.009	0.9968	0.036	1.36	0.00	0.00
	5	20.37	0.007	0.9968	0.042	1.88	0.00	0.00
	6	N/A¥						
	7	N/A¥+						
3	1	20.65	0.0009	0.9928	0.008	0.06	0.00	0.00
	2	20.66	0.004	0.9993	0.014	0.20	0.24	0.48
	3	20.78	0.007	0.9966	0.025	0.63	0.00	0.00
	4	20.71	0.004	0.9870	0.033	1.17	0.00	0.00
	5	20.93	0.0008	0.9913	0.035	1.28	0.00	0.00
	6	N/A¥						
	7	N/A*						

¥ Only mass erosion occurred; run removed from analysis

+ Less than four data points remained in velocity profile after filtration; run removed from analysis

* Flume setting was not reached during testing

Table A.9 Erosion rate and flow data for montmorillonite samples at an average water temperature of 27˚C

Replicate	Flume Setting	Avg water temp, ˚C	Best y_o, mm	Correlation to rough equation	Shear Velocity, u*, m/s	Boundary shear stress, τ_o, Pa	Erosion rate, cm/hr	Er/u*
1	1	27.24	0.0004	0.9809	0.007	0.05	0.00	0.00
	2	27.05	0.014	0.9972	0.017	0.29	0.00	0.00
	3	27.06	0.007	0.9953	0.027	0.74	0.00	0.00
	4	27.04	0.0001	0.9982	0.027	0.74	0.12	0.12
	5	27.04	0.02	0.9984	0.062	4.00	0.12	0.05
	6	27.14	0.05	0.9972	0.089	8.32	0.43	0.14
	7	N/A+						
2	1	27.30	0.0009	0.9943	0.007	0.06	0.48	1.83
	2	27.14	0.003	0.9939	0.013	0.18	0.00	0.00
	3	27.09	0.004	0.9978	0.024	0.61	0.00	0.00
	4	27.06	0.08	0.9857	0.054	3.05	0.12	0.06
	5	27.11	0.007	0.9911	0.043	1.89	0.00	0.00
	6	N/A¥+						
	7	N/A*						
3	1	27.09	0.0008	0.9925	0.008	0.06	0.00	0.00
	2	27.05	0.006	0.9932	0.015	0.25	0.00	0.00
	3	27.06	0.0005	0.9878	0.019	0.39	0.00	0.00
	4	26.90	0.06	0.9848	0.049	2.54	0.00	0.00
	5	N/A¥						
	6	N/A¥						
	7	N/A*						

¥ Only mass erosion occurred; run removed from analysis

\+ Less than four data points remained in velocity profile after filtration; run removed from analysis

* Flume setting was not reached during testing

A.

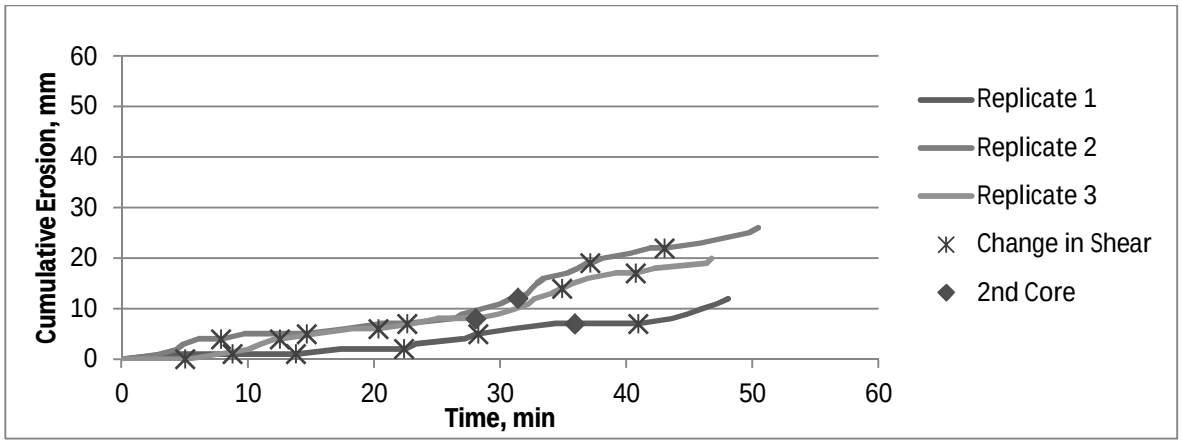

B.

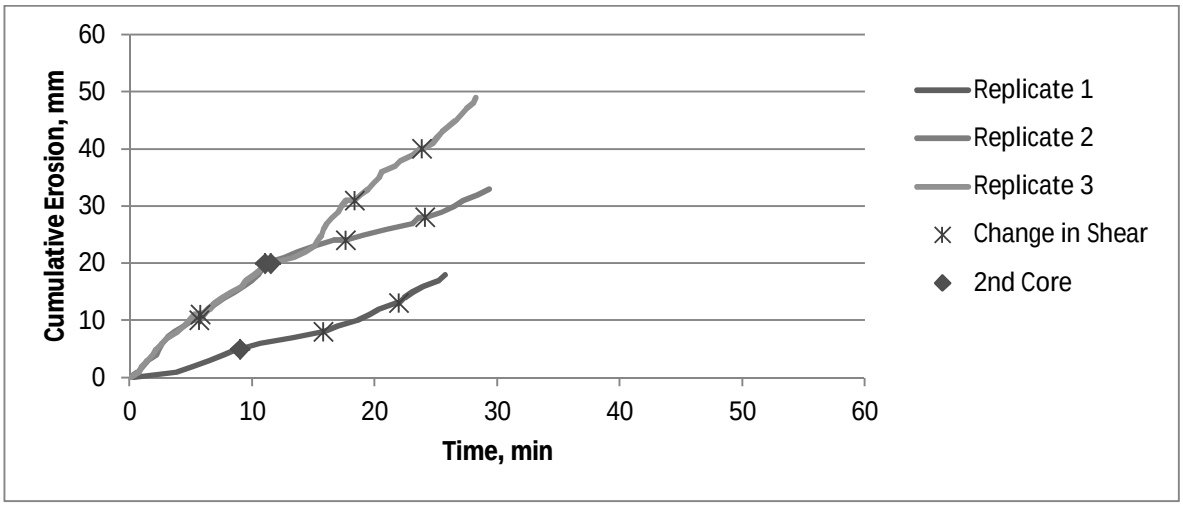

C.

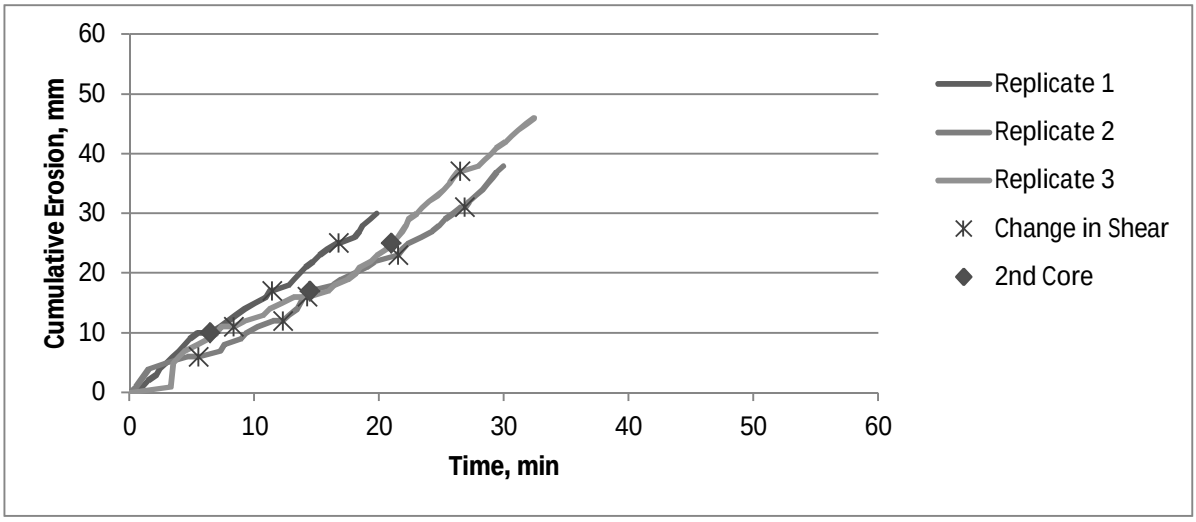

Figure A. 1 Cumulative erosion over time for kaolinite samples for A. 12˚C, B. 20˚C, C. 27˚C; asterisks indicate a change in flume setting, diamonds show when the second core was started

A.

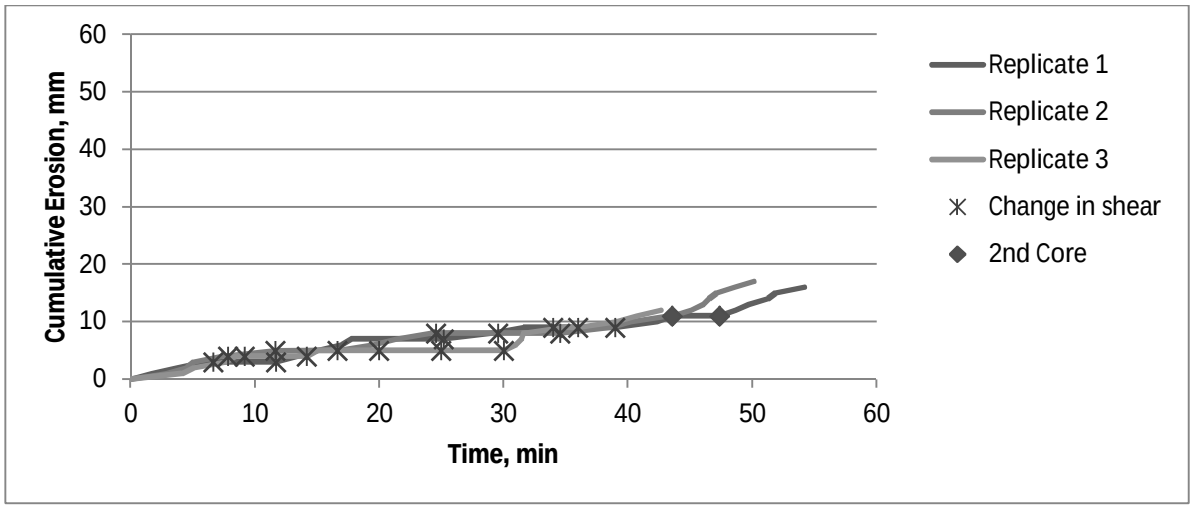

B.

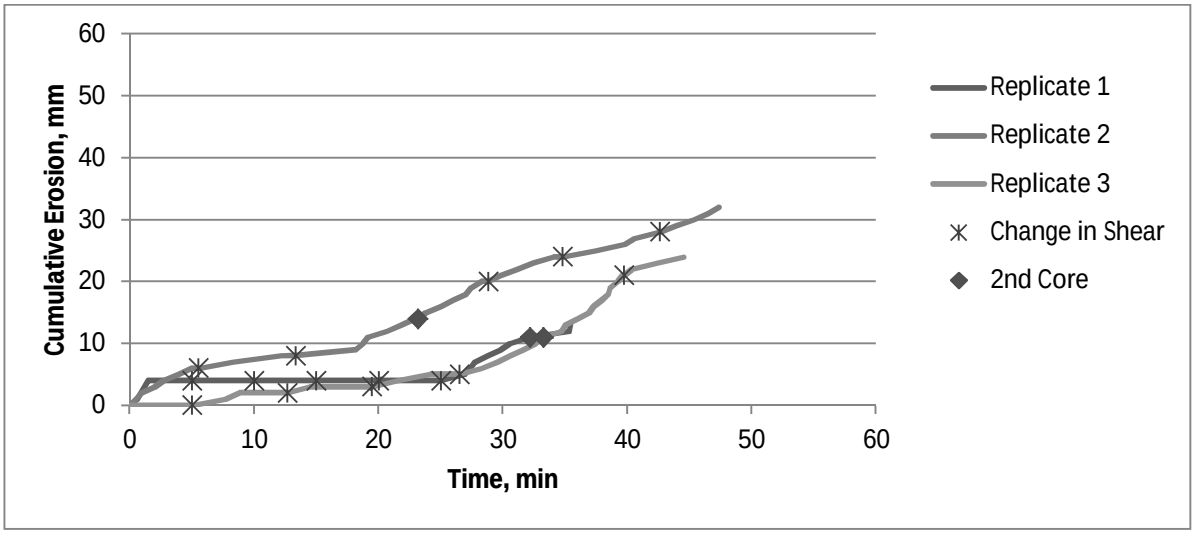

C.

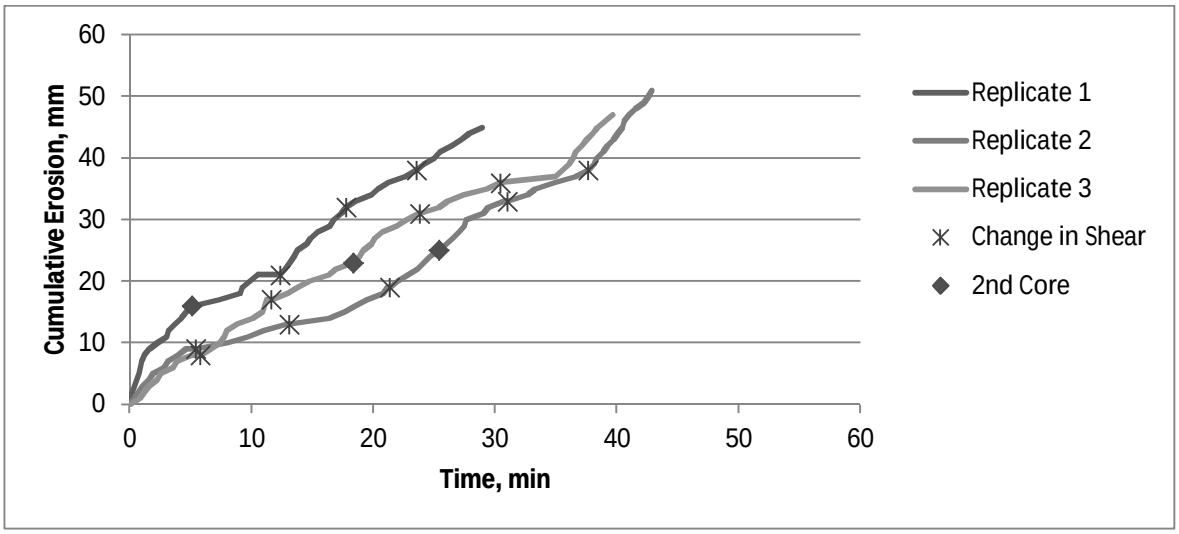

Figure A.2 Cumulative erosion over time for vermiculite samples for A. 12˚C, B. 20˚C, C. 27˚C; asterisks indicate a change in flume setting, diamonds show when the 2nd core was started

A.

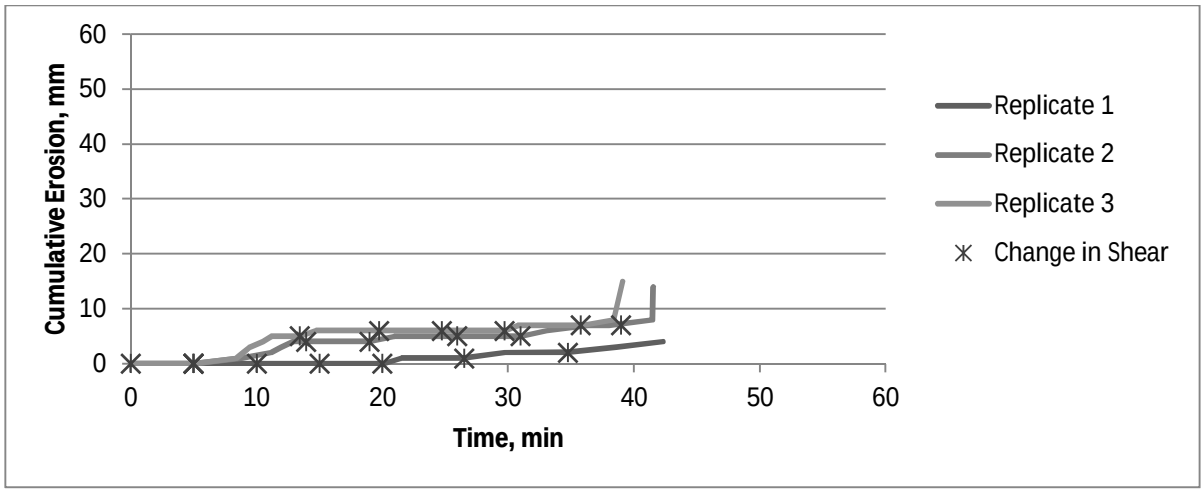

B.

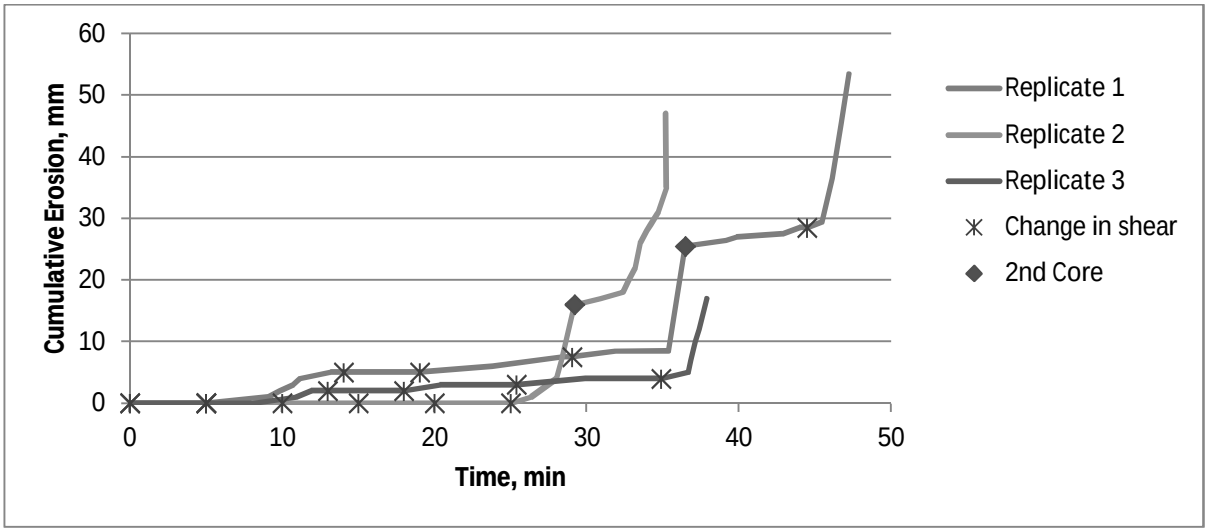

C.

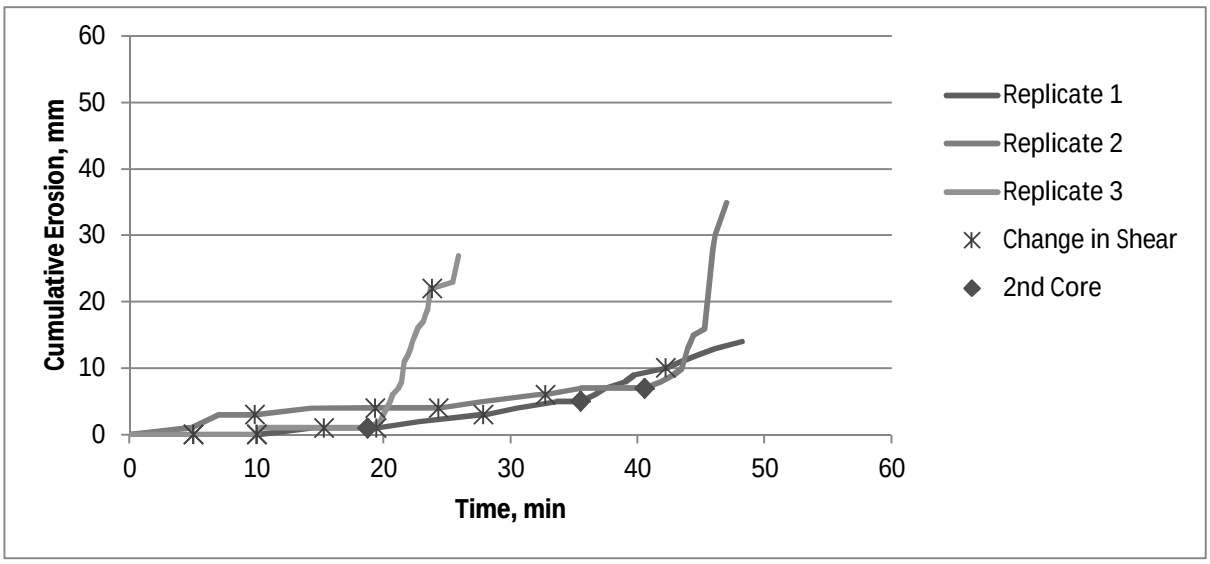

Figure A.3 Cumulative erosion over time for montmorillonite samples for A. 12˚C, B. 20˚C, C. 27˚C; asterisks indicate a change in flume setting, diamonds show when the 2nd core was started

Appendix B Matlab Code for Velocity Profile

```
%% Code to filter velocity data for each soil/temp/rep and save into simpler
file
% Waverly Parks
% June 18, 2012


%% Load and Filter Data
clear
clc
% Load Data File
k=7; %Number of flume settings for the replicate
for i=1:k
run=load(['K101.',num2str(i),'.mat']); %Pick original data file to load
%Set filtration criteria
cor=40;
snr=10;
remove=0.25;

% Data filtration
% Load in vectors to be used for data filtration: SNR and Correlation for
% each APD Beam
SNR1=run.Data.Profiles_SNRBeam1;
SNR2=run.Data.Profiles_SNRBeam2;
SNR3=run.Data.Profiles_SNRBeam3;
SNR4=run.Data.Profiles_SNRBeam4;

COR1=run.Data.Profiles_CorBeam1;
COR2=run.Data.Profiles_CorBeam2;
COR3=run.Data.Profiles_CorBeam3;
COR4=run.Data.Profiles_CorBeam4;

%Set up vectors for binary filtration
[m,n]=size(SNR1);
SNR1F=[m,n];
SNR2F=[m,n];
SNR3F=[m,n];
SNR4F=[m,n];

COR1F=[m,n];
COR2F=[m,n];
COR3F=[m,n];
COR4F=[m,n];

%Filter SNR and Correlation based on criteria: if data point is ok vector
% position is saved as 1, if data point is poor, point is replaced by NaN
for ii=1:n
    for jj=1:m
        if SNR1(jj,ii)<snr
            SNR1F(jj,ii)=NaN;
        else
            SNR1F(jj,ii)=1;
        end
```

```
        if SNR2(jj,ii)<snr
            SNR2F(jj,ii)=NaN;
        else
            SNR2F(jj,ii)=1;
        end

        if SNR3(jj,ii)<snr
            SNR3F(jj,ii)=NaN;
        else
            SNR3F(jj,ii)=1;
        end

        if SNR4(jj,ii)<snr
            SNR4F(jj,ii)=NaN;
        else
            SNR4F(jj,ii)=1;
        end

        if COR1(jj,ii)<cor
            COR1F(jj,ii)=NaN;
        else
            COR1F(jj,ii)=1;
        end

           if COR2(jj,ii)<cor
            COR2F(jj,ii)=NaN;
        else
            COR2F(jj,ii)=1;
           end

           if COR3(jj,ii)<cor
            COR3F(jj,ii)=NaN;
        else
            COR3F(jj,ii)=1;
           end

        if COR4(jj,ii)<cor
            COR4F(jj,ii)=NaN;
        else
            COR4F(jj,ii)=1;
        end

    end
end

% Read in velocity vectors
VX=run.Data.Profiles_VelX; %UP the wall
VY=run.Data.Profiles_VelY; %Stream-wise
VZ1=run.Data.Profiles_VelZ1; %Into stream, perpendicular to wall 1
VZ2=run.Data.Profiles_VelZ2; %Into stream, perpendicular to wall 2

%Filters out bad values based on SNR and Correlation
VXF=VX.*SNR1F.*SNR2F.*SNR3F.*SNR4F.*COR1F.*COR2F.*COR4F.*COR4F;
VYF=VY.*SNR1F.*SNR2F.*SNR3F.*SNR4F.*COR1F.*COR2F.*COR4F.*COR4F;
```

```
VZ1F=VZ1.*SNR1F.*SNR2F.*SNR3F.*SNR4F.*COR1F.*COR2F.*COR4F.*COR4F;
VZ2F=VZ2.*SNR1F.*SNR2F.*SNR3F.*SNR4F.*COR1F.*COR2F.*COR4F.*COR4F;

%Remove Bin of data if more that 15% has been filtered out
BAD=m*remove;
for ii=1:n
        TF=isnan(VXF(:,ii));
        TFsum=sum(TF);
        if TFsum>BAD
            VXF(:,ii)=NaN;
            VYF(:,ii)=NaN;
            VZ1F(:,ii)=NaN;
            VZ2F(:,ii)=NaN;
        end
end

%Average data in each bin
for ii=1:n
    VXavg(i,ii)=nanmean(VXF(:,ii));
    VYavg(i,ii)=nanmean(VYF(:,ii));
    VZ1avg(i,ii)=nanmean(VZ1F(:,ii));
    VZ2avg(i,ii)=nanmean(VZ2F(:,ii));
    VZavg(i,ii)=(VZ2avg(i,ii)+VZ1avg(i,ii))/2;
end

%Get average temperature data
Temp=run.Data.Profiles_Temperature;
Tavg(i)=mean(Temp);

clear run; %clear previous file and variable
clear SNR1 SNR2 SNR3 SNR4 COR1 COR2 COR3 COR4 VXF VYF VZ1F VZ2F VX VY VZ1 VZ2
clear SNR1F SNR2F SNR3F SNR4F COR1F COR2F COR3F COR4F ii jj TF TFsum BAD Temp
end


%Save data into a struct
save('V103RS.mat');
```

Appendix C R Code for Statistical Analysis

Example code to determine mean difference in mean with bootstrap method and the Mann-Whitney t-test between 12→20˚C for kaolinite:

```
#Values are for Kaolinite sample with Er/u*, does not include first shear level
K10<-c(0,0,0.14,0.08,0.11,0,0.16,0.24,0.34,0.07,0.07,0.6,0.13,0.04,0.2,0.07,0.06)
K20<-c(0.54,0.73,0.48,1.21,0.45,0.28,0.29,1.30,1.60,0.77,0.45)
K30<-c(1.12,0.82,0.77,0.92,2.0,0.33,0.37,0.4,0.72,0.84,0.74,0.52)
n<-10000  #number of bootstrap resamplings
Kmean<-numeric(n)  # set up vector to store results
for(i in 1:n){  #loop through each of the resamplings and calculate mean
Kmean[i]<-(mean(sample(K20, replace=T))-mean(sample(K10,replace=T)))
}
hist(Kmean)
quantile(Kmean, 0.05) #Determines lower confidence bound with 95% probability
mean(Kmean) #Displays mean difference in means

#Mann-Whitney t-test
wilcox.test(K10,K20,alt="less")
```

Code to determine correlation between zeta potential and Er/u*:

```
ZK<-c(-0.879, -15.7, -20.7) #Zeta potential and Er/u* for kaolinite
ERK<-c(0.134, 0.737, 0.789)

ZV<-c(-1.189, -21.5, -23.6) #Zeta potential and Er/u* for vermiculite
ERV<-c(0.086, 0.164, 0.749)

ZM<-c(-0.842, -12.2, -12.4) #Zeta potential and Er/u* for montmorillonite
ERM<-c(0.046, 0.135, 0.028)

#Run correlation test for kaolinite
cor.test(ZK, ERK, method="kendall")
cor.test(ZK, ERK, method="spearman")
cor.test(ZK, ERK, method="spearman")
```